Earth Surf. Dynam., 11, 247–257, 2023 https://doi.org/10.5194/esurf-11-247-2023 © Author(s) 2023. This work is distributed under the Creative Commons Attribution 4.0 License.





# Erosion and weathering in carbonate regions reveal climatic and tectonic drivers of carbonate landscape evolution

Richard Ott<sup>1,2</sup>, Sean F. Gallen<sup>3</sup>, and David Helman<sup>4,5</sup>

<sup>1</sup>Department of Earth Sciences, ETH Zurich, Zurich, Switzerland

<sup>2</sup>Earth Surface Geochemistry, GFZ German Research Centre for Geosciences, Potsdam, Germany

<sup>3</sup>Department of Geosciences, Colorado State University, Fort Collins, USA

<sup>4</sup>Department of Soil and Water Sciences, Institute of Environmental Sciences, Faculty of Agriculture,
Food and Environment, The Hebrew University of Jerusalem, Rehovot, Israel

<sup>5</sup>The Advanced School for Environmental Studies, The Hebrew University of Jerusalem, Jerusalem, Israel

Correspondence: Richard Ott (richard.ott@gfz-potsdam.de)

Received: 1 December 2022 – Discussion started: 3 January 2023 Revised: 20 February 2023 – Accepted: 13 March 2023 – Published: 29 March 2023

Abstract. Carbonate rocks are highly reactive and can have higher ratios of chemical weathering to total denudation relative to most other rock types. Their chemical reactivity affects the first-order morphology of carbonate-dominated landscapes and their climate sensitivity to weathering. However, there have been few efforts to quantify the partitioning of denudation into mechanical erosion and chemical weathering in carbonate landscapes such that their sensitivity to changing climatic and tectonic conditions remains elusive. Here, we compile bedrock and catchment-averaged cosmogenic calcite-36Cl denudation rates and compare them to weathering rates derived from stream water chemistry from the same regions. Local bedrock denudation and weathering rates are comparable, 20-40 mm ka <sup>1</sup>, whereas catchment-averaged denudation rates are 2:7 times higher. The discrepancy between bedrock and catchment-averaged denudation is 5 times lower compared to silicate-rich rocks, illustrating that elevated weathering rates make denudation more spatially uniform in carbonatedominated landscapes. Catchment-averaged denudation rates correlate well with topographic relief and hillslope gradients, and moderate correlations with runoff can be explained by concurrent increases in weathering rates. Comparing denudation rates with weathering rates shows that mechanical erosion processes contribute 50 % of denudation in southern France and 70% in Greece and Israel. Our results indicate that the partitioning between largely slope-independent chemical weathering and slope-dependent mechanical erosion varies based on climate and tectonics and impacts the landscape morphology. This leads us to propose a conceptual model whereby in humid, slowly uplifting regions, carbonates are associated with low-lying, flat topography because slopeindependent chemical weathering dominates denudation. In contrast, in arid climates with rapid rock uplift rates, carbonate rocks form steep mountains that facilitate rapid, slope-dependent mechanical erosion required to compensate for inefficient chemical weathering and runoff loss to groundwater systems. This result suggests that carbonates represent an end member for interactions between climate, tectonics, and lithology.

#### 1 Introduction

Landscapes evolve through a combination of mechanical erosion processes and the chemical breakdown of minerals, hereafter referred to as erosion and weathering, respectively (e.g. Gabet and Mudd, 2009). In most silicate-rich landscapes, denudation – the sum of physical erosion and chemical weathering – is dominated by erosion processes (Larsen et al., 2014). In contrast, carbonates are more susceptible to weathering (Gaillardet et al., 1999), likely resulting in a different partitioning of denudation into erosion and weathering for the same climatic and tectonic conditions (Ott et al., 2019). These differences in denudation partitioning should have pronounced effects on landscape morphology, presumably making carbonate landscapes more sensitive to differences in climate than silica bedrock and altering surface and groundwater pathways (e.g. karst hydrology). However, few studies have quantified the relative contributions of erosion and weathering in carbonate-dominated landscapes, the effect of climate and tectonics on such partitioning, and its impact on topography.

The limited number of studies investigating denudation partitioning in carbonates stems largely from challenges in quantifying long-term erosion. Weathering can be constrained by measuring solute fluxes from dissolved loads and direct outcrop measurements with limestone tablets (e.g. Calmels et al., 2014; Goodchild, 1890; Plan, 2005). Denudation, the sum of erosion and weathering, can be quantified using cosmogenic radionuclides (CRNs). These CRNs are produced close to the Earth's surface, and their concentration in surface minerals is inversely proportional to the denudation rate (Lal, 1991). This technique has been widely applied to quartz-bearing rocks. Recent advances in cosmogenic <sup>36</sup>Cl production-rate calibration and calculation (Marrero et al., 2016b; Schimmelpfennig et al., 2009) now allow for the accurate calculation of denudation rates in carbonates at the outcrop and catchment scale. Through the comparison of CRN measurements with weathering rates, it is possible to isolate the contribution of mechanical erosion by subtracting dissolved load-derived weathering from denudation rates (von Blanckenburg et al., 2004; Dixon and Blanckenburg, 2012; Ott et al., 2019), provided that the disparate integration timescales (days to years for weathering rates, thousands of years for CRNs) of each measurement have a negligible impact on measurement comparisons and when CRN weathering biases can be accounted for (Ott et al., 2022; Riebe et al., 2001a). Studies applying a combination of CRN denudation rates and elemental analysis, e.g. measuring concentrations of immobile elements in the bedrock and regolith/saprolite have determined denudation portioning in silicic landscapes (Ferrier et al., 2012; Riebe et al., 2001b, 2003, 2004). However, these combined approaches have not been extended to carbonate landscapes yet.

Studies using CRN or solute flux measurements have arrived at different conclusions regarding carbonate denuda-

tion. Several recent studies assumed that carbonate erosion is negligible even in mountainous landscapes (Avni et al., 2018; Ryb et al., 2014a, b), implying that weathering dominates carbonate denudation budgets. However, other studies found that erosion processes likely play a critical role in carbonate denudation (Covington et al., 2015; Newson, 1971; Ott et al., 2019; Thomas et al., 2017). Here, we contribute to this growing effort by compiling and comparing available cosmogenic calcite-36Cl denudation rate measurements with catchment-averaged weathering rates collected from the same areas to quantify the partitioning between erosion and weathering in carbonate terrains across climatic and tectonic gradients. We use this analysis to illustrate how denudation partitioning varies as a function of climate and tectonics and highlight that carbonate regions are more susceptible to climate-topography interactions than silicate-rich rocks, thus offering the unique potential to identify climate signatures in landscape evolution.

#### 2 Methods

#### 2.1 <sup>36</sup>Cl denudation rate compilation

We compiled 232 bedrock and 43 alluvial sediment <sup>36</sup>Cl measurements from the literature to determine denudation rates at the outcrop and catchment scale, respectively (Fig. 1 and Table S1 in the Supplement). Measurements from alluvial samples were only available from studies around the Mediterranean (Fig. 1). The bedrock denudation rates were sampled from bedrock outcrops or amalgamated clasts on hillslopes or ridgetops, thus recording local bedrock denudation rates. In contrast, the alluvial sediment samples are assumed to be well-mixed and provide a catchment-averaged denudation rate. Published bedrock denudation rates exist for East Asia and the Mediterranean, spanning a range of climate zones from the arid Negev desert in Israel to the humid mountains of Japan, with the mean annual precipitation (MAP) ranging between 190 and 2300 mm a <sup>1</sup>. Alluvial catchments span a narrower range of precipitation rates between 200 and 1100 mm a 1 and drainage areas ranging between a few square kilometres (km<sup>2</sup>) in southern France to tens of square kilometres (km<sup>2</sup>) in Israel and Crete, Greece (see Fig. S1 in the Supplement for catchment maps). Most of the samples in the compilation are from relatively pure, unmetamorphosed to moderately metamorphosed, massive, and bedded limestone bedrock with varying amounts of dolomite (Avni et al., 2018; Godard et al., 2016; Ott et al., 2019; Ryb et al., 2014a, b; Thomas et al., 2017, 2018; Xu et al., 2013). However, the bedrock samples also contain marbles (Matsushi et al., 2010), pure dolostones and chalk (Ben-Asher et al., 2021), and samples of unknown carbonate lithology (Yang et al., 2020).

The calculation of denudation rates from <sup>36</sup>CI concentrations requires knowledge of the chemical composition of the host rock and the so-called target mineral analysed (Schim-

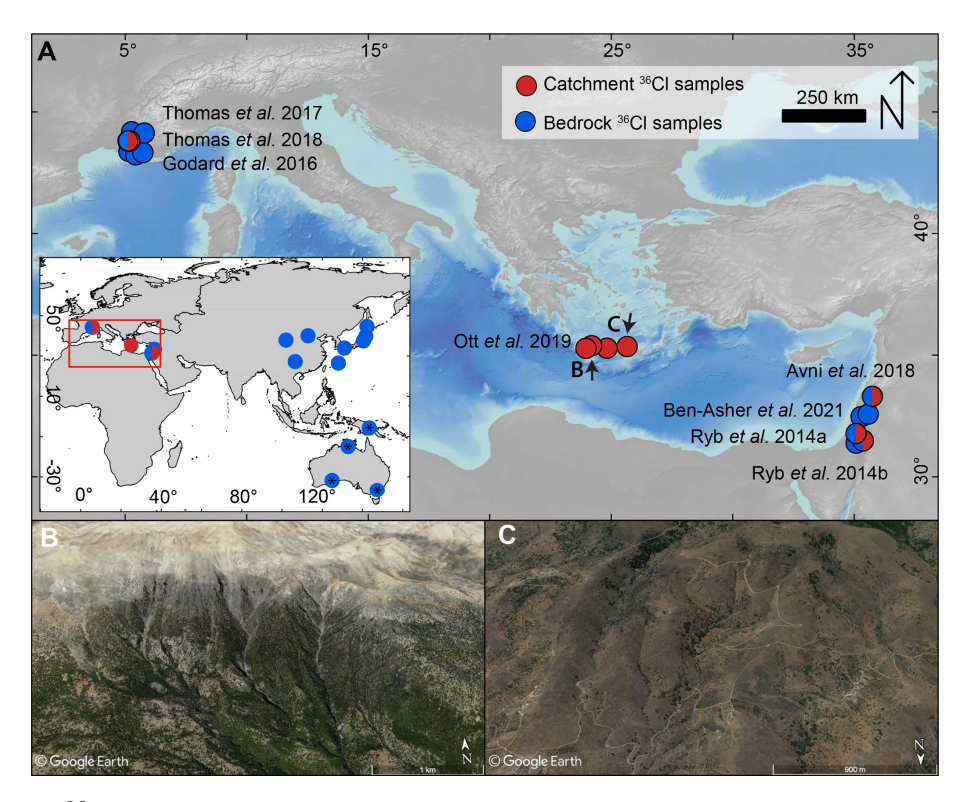


Figure 1. (a) Location of <sup>36</sup>Cl denudation rate measurements compiled for this study in the Mediterranean and globally (inset). Samples not included due to lack of location and compositional data. (b) Typical steep carbonate catchment in the Lefka Ori range in Crete, Greece, with partial forest cover and small landslide scars. (c) Typical low relief catchment in Crete.

melpfennig et al., 2009). To compare denudation rates from different studies, we compiled all chemical sample data from the literature or, if unavailable, contacted the authors (Table S1). Subsequently, all denudation rates were calculated with CRONUScalc v2.1 (Marrero et al., 2016a). Chemical weathering can bias cosmogenic nuclide-derived denudation rates. Weathering in regolith can overestimate <sup>36</sup>Cl denudation rates because the soluble target mineral calcite will have a shorter regolith residence time than the bulk regolith due to its high solubility. We use the methods developed by Ott et al. (2022) to correct all alluvial denudation rates for regolith weathering. However, the difference between weatheringcorrected denudation rates and standard CRONUScalc calculation is generally < 5% (Table S2). Due to the uncertainties in bedrock mineralogy required for accurate weathering corrections, and their low impact on the denudation rate calculation, we present the uncorrected denudation rates in the main text. For more information on the weathering correction of denudation rates, we refer the reader to the Supplement.

#### 2.2 Carbonate weathering rate calculations

We calculated carbonate weathering rates for areas with published catchment-averaged denudation rates to infer the landscape-scale erosion. Erosion can be assumed to equal denudation minus weathering because, despite deep solution features such as caves, volumetrically, most carbonate dissolution occurs close to Earth's surface (Ford and Williams, 2010; Gunn, 2013). Field studies measuring water chemistry at different depths below the surface show that the most weathering occurs within the first metres below the Earth's surface (Gunn, 1981; Williams and Dowling, 1979). Furthermore, studies quantifying the volumetric percentage of voids in carbonate bedrock found that only 0.003 %-0.5 % of the karst volume has been removed by deep dissolution (Worthington and Smart, 2004). Hence, we assume weathering rates primarily reflect near-surface mass removal. In southern France, we used time-averaged water data of [Ca<sup>2C</sup>] and [Mg<sup>2C</sup>] for springs and wells, provided by the national portal of water data (ADES) (Table S3) (Ott et al., 2019). On average, five measurements were available per site, showing only minor variations in [Ca<sup>2C</sup>] and [Mg<sup>2C</sup>] concentrations (Table S3). Therefore, we assume chemostatic behaviour of the carbonate water sources as has been observed for carbonate regions on global and local scales (Bluth and Kump, 1994; Gaillardet et al., 2018; Ott et al., 2019; Zhong et al., 2017). For the catchments in Israel, regional well and spring water chemistry data were published by Ryb et al. (2014b), and in Crete, weathering rates were reported by Ott et al. (2019). All chemical data were corrected for precipitation input by assuming that all [CI ] is derived from precipitation and that other cations are scaled by seawater ratios (Stallard and Ed-

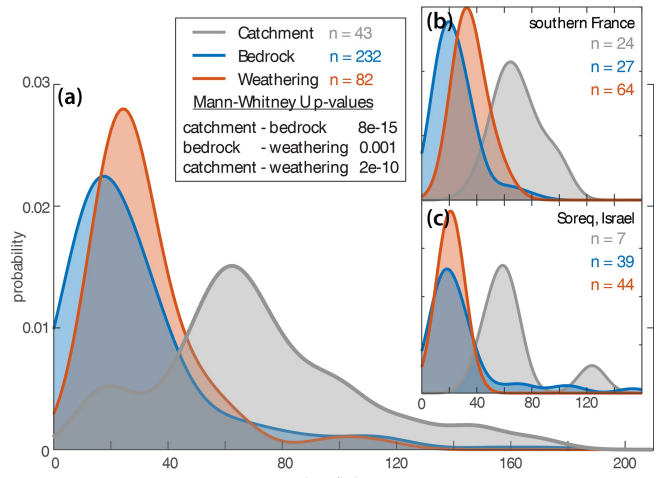


Figure 2. (a) Kernel density plot of weathering, bedrock, and catchment-averaged denudation rates in carbonate catchments for all compiled data. The legend also displays the results from the non-parametric Mann–Whitney U tests, where a low p value indicates a difference in the median value. (b, c) The same plots for south-ern France and the Soreq catchment in Israel; the only two regions where all three data types are available.

mond, 1981). Water data from Israel were not corrected due to unknown [CI ]; however, the correction for  $[Ca^{2C}]$  was usually < 1% and is therefore assumed to be negligible.

To estimate the water flux, we used satellite-derived precipitation and actual evapotranspiration (AET) data. Precipitation was derived from the WorldClim 1km dataset (Fick and Hijmans, 2017) and averaged for each catchment. To determine the runoff available for dissolution, AET was estimated from a parameterization of vegetation indices (PaVI-E) model (Helman et al., 2015) using MODerate resolution Imaging Spectroradiometer (MODIS) satellite data from 2000 to 2016 at 1 km resolution and water vapour flux data from the eddy covariance tower international net (FLUXNET). The PaVI-E was successfully validated against basin-scale AET derived from water balance calculations (i.e. AET D P Q) in the eastern Mediterranean region ( $R^2$  D 0:85, p < 0:05) and was shown to be comparable with other well-established physically-based AET models (Helman et al., 2015, 2017a). It has been used to study climate change impacts on the terrestrial water cycle and is considered a reliable tool for water balance calculations (Helman et al., 2017c, b).

The weathering rate W in mm ka <sup>1</sup> was then calculated by assuming that all [Ca<sup>2C</sup>] and [Mg<sup>2C</sup>] (mg L <sup>1</sup>) in the water are derived from carbonate dissolution and using the water flux from our local runoff calculation (mm ka <sup>1</sup>) for each catchment with the following equation:

where Calcite and Dolomite equals 2.5 and 2.85 gcm 3, respectively. We chose to express the weathering rate as a surface-lowering rate with units of [LT 1] because this is the more common way to quantify denudation rates from cosmogenic nuclides. For groundwater water samples, we estimated a recharge area, equivalent to a groundwater catchment, for runoff averaging based on surface topography and local geology (see Fig. S2 for estimated groundwater recharge areas). Weathering rates were calculated with an uncertainty of 10 % on the precipitation data and 20 % on the actual evapotranspiration. Because recharge areas of springs and wells in karstic terrains can deviate significantly from topographically estimated areas, we calculated a second estimate based on the P and AET average of the entire mountain range where the spring or well is located (Table S3). However, the difference in the average dissolution rate between both approaches is < 3%, and therefore, we choose to use the topographic recharge area estimates outlined in Fig. S2.

#### 2.3 Topographic and climatic metric calculation

Topographic metrics were measured on a 1 arcsec ( 30 m) Shuttle Radar Topography Mission (SRTM) dataset. Slope, mean elevation, mean slope, and mean local relief (500 m radius) were calculated using TopoToolbox (Schwanghart and Scherler, 2014). Analogous to the carbonate weathering rate calculation, the mean annual precipitation (MAP) for catchment-averaged <sup>36</sup>Cl samples was calculated by averaging WorldClim data (Fick and Hijmans, 2017). For locations with catchment-averaged denudation rates, we used our AET estimates to calculate the specific runoff in millimetres per annum (mma <sup>1</sup>) by subtracting MAP from AET values.

#### 3 Results

#### 3.1 Rates of carbonate denudation

Local bedrock denudation rates, as well as weathering rates calculated from water data, are similar and generally fall between 20–40 mm ka <sup>1</sup> (mean 1: 29 25 and 32 19 mm ka <sup>1</sup>, respectively) (Fig. 2). In contrast to the lo-cal bedrock denudation rates, catchment-averaged denudation rates from alluvial samples are 2:7 times higher than weathering rates (mean 81 35 mm ka <sup>1</sup>) (Fig. 2). A Mann–Whitney U test shows that distributions of weather-ing, bedrock, and catchment-averaged rate are statistically different at > 99 % confidence (Fig. 2a). The trends from the

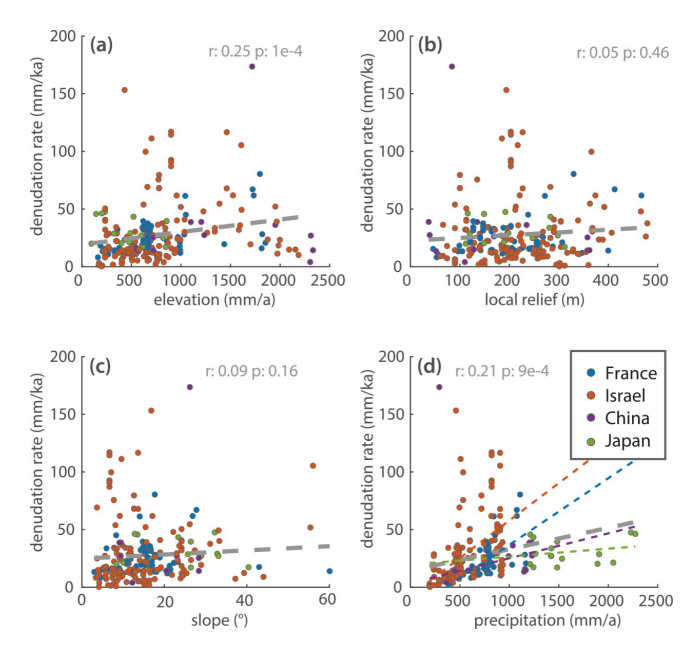


**Figure 3.** Correlation between <sup>36</sup>Cl bedrock denudation rates, to-pographic metrics, and mean annual precipitation (MAP) based on linear regression. Colours indicate different sample locations; Pearson's r values and p values for the regressions are displayed. In panel (d), region-specific positive relationships with MAP exist and are highlighted.

global dataset can also be observed on the local scale where climatic and lithologic conditions are more uniform (Fig. 2b and c). In the Soreq catchment in Israel, and the carbonate mountain ranges of southern France, bedrock and weathering rates are similar, and catchment-averaged denudation rates are substantially higher.

#### 3.2 Carbonate denudation and weathering rates as a function of topographic and climatic factors

Correlations between the local bedrock denudation rate and topographic and climatic variables are weak (Pearson's r < 0:25) (Fig. 3). Some region-specific local bedrock denudation rates show positive relationships with MAP (Fig. 3d). However, the covariation of topographic metrics and precipitation (Pearson's r generally > 0:5, Tables S5 and S6) associated with orography impedes isolating climatic effects from these correlations. Unfortunately, AET data were not available for several bedrock sampling locations, and therefore no comparison with runoff could be performed.

Catchment-averaged denudation rates show strong-to-moderate correlations with topographic metrics such as local relief and slope (Pearson's r of 0.65 and 0.5, respectively, Fig. 4a and b). Catchment-averaged rates also scale strongly with precipitation; however, all study sites exhibit orographic precipitation gradients such that precipitation is correlated with topography (Fig. 4c inset). However, when comparing denudation rates to runoff, the correlation is weak (r D 0:38).

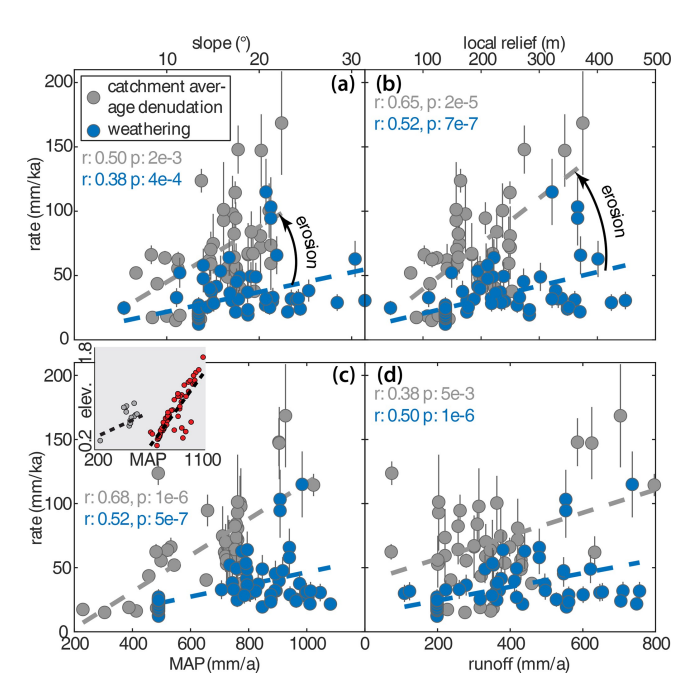


Figure 4. Correlations between catchment average <sup>36</sup>Cl denudation rates, carbonate weathering rates, and topographic and climatic metrics based on linear regression. Values of correlation coefficient and p value displayed for catchment-averaged denudation and weathering rates. Inset (c): Correlation between mean annual precipitation (MAP) and elevation illustrating orographic precipitation in the analysed areas (Israel, grey; France and Crete, red).

The slopes of the regression lines for catchment-averaged denudation and weathering rates are similar (Fig. 4d). Weathering rates show weak-to-moderate correlations with topographic and climatic variables but remain consistently lower than catchment-averaged denudation rates across all variable gradients. The same trends can also be observed on a local scale. Crete is the only region where samples cover significant gradients of all analysed metrics, and generally the correlations are similar to Fig. 4 (Fig. S3).

#### 4 Discussion

#### 4.1 Rates of carbonate bedrock denudation

The similarity of denudation rates for outcrops and weathering suggests that weathering may be the dominant denudation process for locally exposed bedrock on hillslopes. This has also been suggested based on the observations of outcrops with micro-erosion metres (Cucchi et al., 1996; Furlani et al., 2009). However, due to the difference in the spatial scale of catchment weathering rates and local bedrock denudation rates, this link remains vague. The large scatter in the relationship between bedrock denudation rates and topographic and climatic variables is likely related to a number of site-specific factors that cannot be accounted for in a large-scale compilation. Though all samples are from car-

bonate bedrock, likely significant variations in mineralogy, diagenesis, and bedding structure exist, which may have a strong influence on the resulting denudation rate. Additionally, the topographic variables were measured at 30 m resolution, which only gives a rough estimate of the local slope for a bedrock sample. The exact geomorphic position of bedrock samples is likely to be very important for the measured denudation rate and cannot be resolved within this dataset. Moreover, the at-a-site variations in bedrock denudation rates are commonly large (e.g. Avni et al., 2018; Ryb et al., 2014b), suggesting that small-scale variability is high and hinders the observation of clear trends. Thus, our further analysis of climatic and tectonic controls focuses primarily on the catchment-averaged samples.

## 4.2 Discrepancy between bedrock and catchment-wide denudation rates

Analogous to our findings, a discrepancy between bedrock and catchment-averaged denudation rates has also been documented in a compilation of silicate-rich rock units (Portenga and Bierman, 2011). This difference has been interpreted as reflecting growing topographic relief because rivers are thought to erode faster than the ridgelines (Hancock and Kirwan, 2007; Small and Anderson, 1998; Thomas et al., 2017) or higher weathering rates below soil-covered bedrock and therefore a sampling bias toward fresh outcrop surfaces (Portenga and Bierman, 2011). It seems unlikely that all studies comparing bedrock interfluve samples and catchment averages would find increasing relief, and therefore another explanation is needed. If the rate discrepancy is due to soil cover, measured soil production rates should equal the catchment-averaged rates. Yet, a global compilation of soil production rates shows that most measurements are significantly lower than the catchment-averaged denudation rates (Heimsath et al., 2012). An alternative explanation is that both local bedrock denudation and soil production rates, whether in carbonates or siliciclastic rocks, represent a biased sampling of stable portions of the landscape (e.g. areas not affected by recent mass wasting). Catchment-averaged sampling incorporates all portions of the upstream landscape and reflects a mix between the local high denudation rate associated with mass wasting and a "background" rate set by bedrock denudation and soil production.

In silicate-rich regions, catchment-averaged denudation rates are between 10 (median) and 20 times (mean) higher than bedrock denudation (Portenga and Bierman, 2011). The smaller 2:7-fold discrepancy between local bedrock and catchment-averaged rates in carbonate terrains is best explained by the elevated role of chemical weathering in carbonates (> 1=3 of denudation, Fig. 3) compared to silica-rich rocks (< 5 % of denudation) (Larsen et al., 2014). This result implies that carbonate regions have more uniform lowering rates due to weathering compared to silicate-rich landscapes. Below, we discuss how these findings have important impli-

cations for landscape evolution in carbonates and their topographic response to tectonic uplift and climate because erosion is slope-dependent, whereas weathering mostly depends on climate and vegetation (Gaillardet et al., 2018).

#### 4.3 Mechanical erosion in carbonate landscapes

We consider three possible explanations for the 2-3fold difference between catchment-scale weathering rates and catchment-averaged denudation rates: (1) catchmentaveraged rates overestimate denudation due to low <sup>36</sup>Cl concentration material from deep landslides (> 5 m, Yanites et al., 2009); (2) higher runoff earlier in the averaging time window of cosmogenic nuclides (Ryb et al., 2014b, 2015); (3) mechanical denudation of carbonates. A deep-seated landslide bias seems unlikely due to the consistent discrepancy between catchment-averaged denudation and weathering in a diverse array of topography, from low relief and slope areas in Israel to the rugged mountainous terrain of Crete (Figs. 1 and 2). Furthermore, most sampled catchments drain moderately sized areas (tens of square kilometres) and are therefore large enough to buffer potential biases arising from mass wasting (Niemi et al., 2005; Schide et al., 2022; Yanites et al., 2009).

The disparate integration timescales of cosmogenic nuclide (10<sup>2</sup>–10<sup>5</sup> years) and weathering rate measurements (0– 10<sup>2</sup> years) led Ryb et al. (2014b, 2015) to suggest that higher CRN-derived catchment-averaged denudation rates integrated a history of more vigorous weathering associated with past wetter climates. Most of the compiled catchmentaveraged denudation rates reflect time-integrated rates from the modern to mid-Holocene, with the lowest rates integrating timescales to the last glacial maximum (LGM). To test this hypothesis, we compared current precipitation to 1 km resolution WorldClim paleo-precipitation maps from three different climate models (Fick and Hijmans, 2017). We found that precipitation was 2% to 27% higher in the mid-Holocene compared to the modern era and between 25 % drier or 55% wetter in the LGM, depending on the area and preferred model in the three Mediterranean sampling areas (Fig. 5). Since weathering scales linearly with the water availability (White, 1984), these changes in precipitation, even with a total drawdown of actual evapotranspiration, cannot explain the data discrepancy through an increased paleowater flux when integrated over time.

Overall, these observations suggest that in Mediterranean carbonate landscapes, mechanical erosion contributes significantly to denudation because (1) catchment-averaged denudation rates are substantially higher than weathering rates; (2) denudation rates scale with topographic steepness, which is expected for gravity-driven erosion processes; (3) the difference between denudation and weathering, which we interpret as erosion, also increases with increasing topographic steepness (Fig. 4); whereas (4) the parallel trends of denudation and weathering with runoff suggest that the scaling of

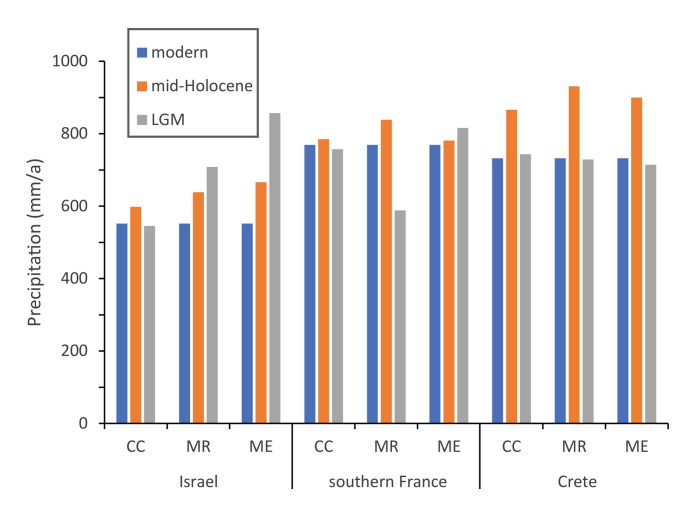


Figure 5. Comparison of modern and paleo-precipitation rates from climate models for all areas with published catchment-averaged denudation rates. For three different WorldClim paleo-climate models (CC, MR, ME) (Fick and Hijmans, 2017), paleo-precipitation values were extracted for all sampled <sup>36</sup>Cl sampling locations, averaged for each region and compared to modern precipitation rates. LGM – last glacial maximum.

denudation with runoff can be accounted for by increased weathering (Fig. 4d).

# 4.4 Landscape evolution in carbonates compared to other rock types

Averaging catchment-averaged denudation and weathering rates for southern France, Israel (Soreg), and Crete, we find erosion-to-weathering ratios of 1.0, 2.2, and 2.5, respectively (Fig. 6). The substantial amount of erosion in these carbonate landscapes requires steep, high relief topography allowing slope-dependent processes to thrive. Carbonate weathering rates are largely dependent on water flux, temperature, and vegetation (Atkinson and Smith, 1976; Gaillardet et al., 2018) and can therefore be seen as a proxy for climate. Denudation rates typically evolve to balance tectonic uplift and can be viewed as a tectonic proxy. Carbonates in slowly uplifting areas will denude sluggishly. Under favourable climatic conditions, weathering alone is sufficient to balance rock uplift with little need for the development of steep topography to enhance erosion rates. This conceptual model explains why carbonates remain topographically subdued under certain conditions. Less-soluble lithologies will stick out because surface-lowering can only be achieved through erosion, requiring local slopes to form. This end member can be observed in Ireland or the Appalachians, where carbonates denude mostly through dissolution, and eroding sandstone ridges form the topographic highs (Duxbury et al., 2015; Simms, 2004), though some of the topographic features in Ireland may have been overprinted by Quaternary glaciations.

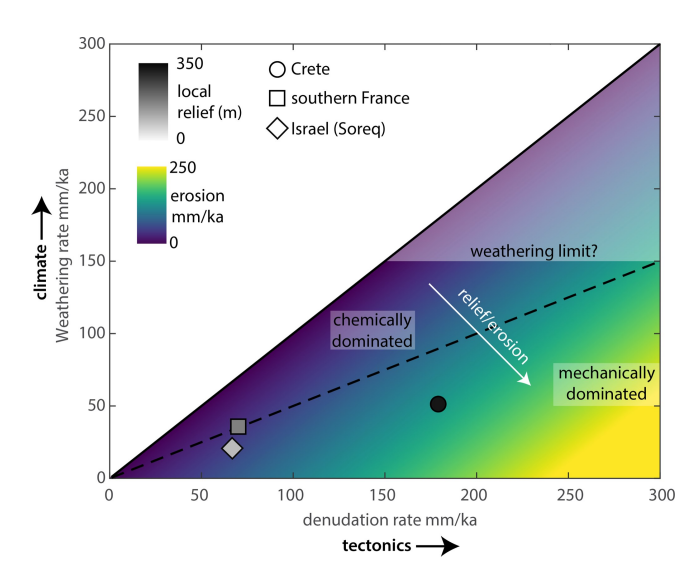


Figure 6. Mean weathering versus mean denudation rates for the sites with alluvial denudation data. The dashed line is the 1 V1 ratio of weathering and erosion. Weathering-dominated landscapes will tend to be subdued; high erosion rates will lead to high relief areas dominated by slope-dependent mechanical processes.

The local climate will mainly set the weathering rate. Still, it may be subject to a dissolution speed limit because of the following: (1) a chemical threshold of  $< 200 \,\mathrm{mg}\,\mathrm{L}^{-1}$  water hardness, which has been observed globally (Covington et al., 2015; Gaillardet et al., 2018), (2) an increase in precipitation will typically be partially compensated by an increased AET, and (3) tropical regions with high runoff have lower water hardness due to a decrease in carbonate solubility with temperature (Atkinson and Smith, 1976; Gaillardet et al., 2018). A global compilation of carbonate weathering rates finds a maximum rate of 140 mm ka 1 (Gaillardet et al., 2018), similar to our highest rate of 115 mm ka <sup>1</sup>. These rates may represent a carbonate weathering speed limit beyond which local uplift cannot be accommodated; this is when erosion becomes dominant and topography steepens (Fig. 6). Erosion is thought to accelerate weathering by breaking rocks down and increasing surface area (e.g. Rinder and von Hagke, 2021), resulting in a direct feedback between erosion and weathering. In silicate-rich rocks, this has been shown to be true for low and moderate denudation rates, with a transition to a climate limit at high denudation rates (Bufe et al., 2021; West et al., 2005). However, some observations suggest that the feedback between erosion and weathering rate is weak or nonexistent in carbonates. Long-term weathering rates of carbonates in experiments were independent of grain size and texture (Levenson et al., 2015). Additionally, water chemistry measurements that suggest carbonate weathering is generally limited by water and acid availability (Bufe et al., 2021), except for regions where carbonates are a minor component of the bedrock or denudation, increases the acid supply (Bufe et al., 2021; Erlanger et al., 2021).

In carbonate regions where mechanical erosion prevails, the formation of karst features will cause surface water infiltration and lower the discharge of surface streams. Reduction in stream discharge will decrease the erosional efficiency and cause steepening of the landscape compared to regions with less-soluble bedrock (Ott et al., 2019). This explains why carbonate terrain in locations with arid to semi-arid climates and significant uplift rates form steeper topography than areas underlain by silicate-rich lithologies (Ott, 2020; Ott et al., 2019), and carbonates form the low parts of the landscape, e.g. in Ireland or the Appalachians, where uplift rates are low, and the climate is favourable for weathering (Gallen, 2018). Undoubtedly, feedbacks may exist where mountain building causes more orographic precipitation, as seen in the Mediterranean study sites, which increases weathering. Therefore, the climate and tectonic axis in Fig. 6 should not necessar-ily be seen as entirely independent. Additionally, Erlanger et al. (2021) showed that significant amounts of dissolved load could reprecipitate as secondary calcite in rivers flow-ing through carbonates since soil pore water equilibrated to high CO<sub>2</sub> levels degasses upon entering streams. This effect has not been observed in the ephemeral catchments studied here but shows how erosion and weathering can be linked in wetter regions, and catchment and local-scale weathering rates may differ.

Our results have important implications for landscape evolution. The difference in denudation partitioning compared to silicate-rich rocks makes the topography of carbonate regions more sensitive to the interplay of tectonics and climate. Studies investigating the climatic and tectonic effects on topography typically report that tectonics govern the first-order landscape morphology (Seybold et al., 2021). However, in mountain belts with a lot of exposed carbonate bedrock, the topographic expression could be different from silicatedominated mountains. Indeed, studies of the relationship between bedrock channel steepness and erosion rate or rock uplift rate show that the functional form of these parameters is different between silica- and carbonate-rich bedrock. Stud-ies of bedrock rivers in silica-rich rock generally show chan-nel steepness - erosion rate relationships are described by a power function with an exponent n between 1:5–3 (DiB-iase et al., 2010; Harel et al., 2016; Ouimet et al., 2009). In contrast, similar studies in carbonate-rich bedrock channels find that this exponent n is 0:5 (Attal et al., 2011; Gallen and Wegmann, 2017; Royden and Taylor Perron, 2013; Whit-taker et al., 2008). The implication of these results is that as channels steepen, bulk erosional efficiency increases in silicia-rich bedrock, whereas in carbonate-rich bedrock, it declines. These contrasting behaviours are perhaps related to surface water infiltration associated with the high reactivity of carbonates relative to silica-rich rock, but the exact causal mechanisms are currently unknown (Gallen and Wegmann, 2017).

These behaviours and the sensitivity to environmental variables could be investigated by studying topography, to-

gether with erosion and weathering rates in carbonate regions along climatic and tectonic gradients. Such studies could benefit from the recently developed <sup>10</sup>Be-<sup>36</sup>Cl paired nuclide approach by Ott et al. (2022) that can be used to determine long-term erosion and weathering rates from the same sample. We also speculate that the chemical threshold of carbonate weathering and runoff loss due to surface water infiltration in carbonate regions might cause non-linear topographic responses to climate and tectonic forcing. Many of these hypotheses can be tested with future studies that fill the climatic–tectonic parameter space in Fig. 6. Hence, we argue that the reactive nature of carbonate regions offers the potential to observe strong controls of climate responses to tectonics on landscape evolution, and carbonate-dominated mountain belts should be targeted in future work.

#### 5 Summary and conclusions

We compiled all available <sup>36</sup>Cl denudation rate measurements from carbonate regions and compared them to weathering rates. Our main findings are as follows:

- 1. The range of bedrock denudation and weathering rates are similar and range between 20–40 mm ka<sup>-1</sup>, suggesting that weathering may be the main process of lowering at the bedrock sampling scale. Catchment-wide denudation rates are on average 2.7 times higher, resembling the incorporation of all denudation processes in the catchment.
- The discrepancy between bedrock and catchment-wide denudation rates in carbonates is 5 times lower than in silicate-rich rocks, reflecting a higher weatherability and suggesting more uniform landscape lowering.
- 3. Denudation rates are higher than weathering rates, and the differences increase with topographic steepness. This suggests substantial mechanical erosion in carbonate regions, which we estimate to be between 50%— 70% of denudation in the sampled Mediterranean regions.
- 4. In regions where uplift rates are low, denudation is mostly achieved through weathering, carbonates will form the low part of the landscape, because no slopes need to be formed for denudation. However, in regions of higher uplift, erosion needs to occur, which requires slopes to form. In these regions, infiltration commonly lowers the efficiency of surface processes, thereby steepening the carbonate parts of the landscape. Hence, depending on the partitioning of denudation into weathering and erosion, carbonates form either the steep or the low part of landscape compared to silicate-rich rocks.

Data availability. All data required to reproduce the study are reported within the main text and the Supplement.

**Supplement.** The supplement related to this article is available online at: https://doi.org/10.5194/esurf-11-247-2023-supplement.

**Author contributions.** RO: conceptualization, funding acquisition, investigation, data curation, writing — original draft preparation; SFG: conceptualization, funding acquisition, writing — review and editing; DH: methodology, writing — review and editing.

Competing interests. The contact author has declared that none of the authors has any competing interests.

Disclaimer. Publisher's note: Copernicus Publications remains neutral with regard to jurisdictional claims in published maps and institutional affiliations.

Acknowledgements. Sean F. Gallen was partially supported by the NSF awards EAR-1945970, EAR-2041910, and EAR-2139894 and funds were provided by the Colorado State University.

Financial support. This research has been supported by the Horizon Europe Marie Skłodowska-Curie Actions (grant no. 674899) and the Schweizerischer Nationalfonds zur Förderung der Wissenschaftlichen Forschung (grant no. P2EZP2 191866).

**Review statement.** This paper was edited by Robert Hilton and reviewed by Aaron Bufe and one anonymous referee.

#### References

- Atkinson, T. C. and Smith, D. I.: The erosion of limestones, edited by: Ford, T. D. and Cullingford, C. H. D. M.-C., Academic Press, London, 151–171, 1976.
- Attal, M., Cowie, P. A., Whittaker, A. C., Hobley, D., Tucker, G. E., and Roberts, G. P.: Testing fluvial erosion models us-ing the transient response of bedrock rivers to tectonic forc-ing in the Apennines, Italy, J. Geophys. Res.-Earth, 116, 2005, https://doi.org/10.1029/2010JF001875, 2011.
- Avni, S., Joseph-Hai, N., Haviv, I., Matmon, A., Benedetti, L., and ASTER team: Patterns and rates of 103–105 yr denudation in carbonate terrains under subhumid to subalpine climatic gradient, Mount Hermon, Israel, Geol. Soc. Am. Bull., 131, 899–912, https://doi.org/10.1130/B31973.1, 2018.
- Ben-Asher, M., Haviv, I., Crouvi, O., Roering, J. J., and Matmon, A.: The convexity of carbonate hilltops: <sup>36</sup>Cl constraints on denudation and chemical weathering rates and implications for hillslope curvature, GSA Bull., 133, 1930–1946, https://doi.org/10.1130/B35658.1, 2021.

- Bluth, G. J. S. and Kump, L. R.: Lithologic and climatologic controls of river chemistry, Geochim. Cosmochim. Ac., 58, 2341–2359, https://doi.org/10.1016/0016-7037(94)90015-9, 1994.
- Bufe, A., Hovius, N., Emberson, R., Rugenstein, J. K. C., Galy, A., Hassenruck-Gudipati, H. J., and Chang, J. M.: Co-variation of silicate, carbonate and sulfide weathering drives CO<sub>2</sub> release with erosion, Nat. Geosci., 14, 211–216, https://doi.org/10.1038/s41561-021-00714-3, 2021.
- Calmels, D., Gaillardet, J., and François, L.: Sensitivity of carbonate weathering to soil CO<sub>2</sub> production by biological activity along a temperate climate transect, Chem. Geol., 390, 74–86, https://doi.org/10.1016/j.chemgeo.2014.10.010, 2014.
- Covington, M. D., Gulley, J. D., and Gabrovšek, F.: Natural variations in calcite dissolution rates in streams: Controls, implications, and open questions, Geophys. Res. Lett., 42, 2836–2843, https://doi.org/10.1002/2015GL063044, 2015.
- Cucchi, F., Marinetti, E., and Forti, F.: Surface degradation of carbonate rocks in the karst of Trieste (Classical Karst, Italy), Karren landforms Proc. Int. Symp. Karren Landforms, Sóller, 19–24 September 1995, 41–52, ISBN 84-7632-297-6, 1996.
- DiBiase, R. A., Whipple, K. X., Heimsath, A. M., and Ouimet, W. B.: Landscape form and millennial erosion rates in the San Gabriel Mountains, CA, Earth Planet. Sc. Lett., 289, 134–144, https://doi.org/10.1016/j.epsl.2009.10.036, 2010.
- Dixon, J. L. and Blanckenburg, F.: Soils as pacemakers and limiters of global silicate weathering, CR Geosci., 344, 597–609, https://doi.org/10.1016/j.crte.2012.10.012, 2012.
- Duxbury, J., Bierman, P. R., Portenga, E. W., Pavich, M. J., Southworth, S., and Freeman, S. P. H. T.: Erosion rates in and around Shenandoah National Park, Virginia, determined using analysis of cosmogenic <sup>10</sup>Be, Am. J. Sci., 315, 46–76, https://doi.org/10.2475/01.2015.02, 2015.
- Erlanger, E. D., Rugenstein, J. K. C., Bufe, A., Picotti, V., and Willett, S. D.: Controls on Physical and Chemical Denudation in a Mixed Carbonate-Siliciclastic Orogen, J. Geophys. Res.-Earth, 126, e2021JF006064, https://doi.org/10.1029/2021JF006064, 2021.
- Ferrier, K. L., Kirchner, J. W., and Finkel, R. C.: Weak influences of climate and mineral supply rates on chemical erosion rates: Measurements along two altitudinal transects in the Idaho Batholith, J. Geophys. Res.-Earth, 117, 2026, https://doi.org/10.1029/2011JF002231, 2012.
- Fick, S. E. and Hijmans, R. J.: WorldClim 2, Int. J. Climatol., 37, 4302–4315, https://doi.org/10.1002/joc.5086, 2017.
- Ford, D. and Williams, P. W.: Karst hydrogeology and geomorphology, rev. edn., John Wiley & Sons, Chichester, England, A Hoboken, NJ, https://doi.org/10.1002/9781118684986, 2010.
- Furlani, S., Cucchi, F., Forti, F., and Rossi, A.: Comparison between coastal and inland Karst limestone lowering rates in the northeastern Adriatic Region (Italy and Croatia), Geomorphology, 104, 73–81, https://doi.org/10.1016/j.geomorph.2008.05.015, 2009.
- Gabet, E. J. and Mudd, S. M.: A theoretical model coupling chemical weathering rates with denudation rates, Geology, 37, 151–154, https://doi.org/10.1130/G25270A.1, 2009.
- Gaillardet, J., Dupré, B., Louvat, P., and Allègre, C. J.: Global silicate weathering and CO<sub>2</sub> consumption rates deduced from the chemistry of large rivers, Chem. Geol., 159, 3–30, https://doi.org/10.1016/S0009-2541(99)00031-5, 1999.

- Gaillardet, J., Calmels, D., Romero-Mujalli, G., Zakharova, E., and Hartmann, J.: Global climate control on carbonate weathering intensity, Chem. Geol., 527, 118762, https://doi.org/10.1016/j.chemgeo.2018.05.009, 2018.
- Gallen, S. F.: Lithologic controls on landscape dynamics and aquatic species evolution in post-orogenic mountains, Earth Planet. Sc. Lett., 493, 150–160, https://doi.org/10.1016/j.epsl.2018.04.029, 2018.
- Gallen, S. F. and Wegmann, K. W.: River profile response to normal fault growth and linkage: an example from the Hellenic forearc of south-central Crete, Greece, Earth Surf. Dynam., 5, 161–186, https://doi.org/10.5194/esurf-5-161-2017, 2017.
- Godard, V., Ollivier, V., Bellier, O., Miramont, C., Shabanian, E., Fleury, J., Benedetti, L., and Guillou, V.: Weathering-limited hill-slope evolution in carbonate landscapes, Earth Planet. Sc. Lett., 446, 10–20, https://doi.org/10.1016/j.epsl.2016.04.017, 2016.
- Goodchild, J. G.: VIII. Notes on some Observed Rates of Weathering of Limestones, Geol. Mag., 7, 463–466, 1890.
- Gunn, J.: Limestone solution rates and processes in the Waitomo District, New Zealand, Earth Surf. Proc. Land., 6, 427–445, https://doi.org/10.1002/esp.3290060504, 1981.
- Gunn, J.: 6.7 Denudation and Erosion Rates in Karst, in: Treatise on Geomorphology, edited by: Shroder, J. F., Academic Press, 72–81, ISBN 9780080885223, https://doi.org/10.1016/B978-0-12-374739-6.00115-9, 2013.
- Hancock, G. and Kirwan, M.: Summit erosion rates deduced from <sup>10</sup>Be: Implications for relief production in the central Appalachians, Geology, 35, 89, https://doi.org/10.1130/G23147A.1, 2007.
- Harel, M. A., Mudd, S. M., and Attal, M.: Global analysis of the stream power law parameters based on worldwide <sup>10</sup>Be denudation rates, Geomorphology, 268, 184–196, https://doi.org/10.1016/j.geomorph.2016.05.035, 2016.
- Heimsath, A. M., DiBiase, R. A., and Whipple, K. X.: Soil production limits and the transition to bedrock-dominated landscapes, Nat. Geosci., 5, 210–214, https://doi.org/10.1038/ngeo1380, 2012.
- Helman, D., Givati, A., and Lensky, I. M.: Annual evapotranspiration retrieved from satellite vegetation indices for the eastern Mediterranean at 250 m spatial resolution, Atmos. Chem. Phys., 15, 12567–12579, https://doi.org/10.5194/acp-15-12567-2015, 2015.
- Helman, D., Lensky, I. M., Osem, Y., Rohatyn, S., Rotenberg, E., and Yakir, D.: A biophysical approach using water deficit factor for daily estimations of evapotranspiration and CO<sub>2</sub> uptake in Mediterranean environments, Biogeosciences, 14, 3909–3926, https://doi.org/10.5194/bg-14-3909-2017, 2017a.
- Helman, D., Lensky, I. M., Yakir, D., and Osem, Y.: Forests growing under dry conditions have higher hydrological resilience to drought than do more humid forests, Global Change Biol., 23, 2801–2817, https://doi.org/10.1111/gcb.13551, 2017b.
- Helman, D., Osem, Y., Yakir, D., and Lensky, I. M.: Relationships between climate, topography, water use and productivity in two key Mediterranean forest types with different water-use strategies, Agr. Forest Meteorol., 232, 319–330, https://doi.org/10.1016/j.agrformet.2016.08.018, 2017c.
- Lal, D.: Cosmic ray labeling of erosion surfaces: in situ nuclide production rates and erosion models, Earth Planet. Sc. Lett., 104, 424–439, https://doi.org/10.1016/0012-821X(91)90220-C, 1991.

- Larsen, I. J., Almond, P. C., Eger, A., Stone, J. O., Montgomery, D. R., and Malcolm, B.: Rapid soil production and weather-ing in the Southern Alps, New Zealand, Science, 343, 637–640, https://doi.org/10.1126/science.1244908, 2014.
- Levenson, Y., Schiller, M., Kreisserman, Y., and Emmanuel, S.: Calcite dissolution rates in texturally diverse calcareous rocks, Geol. Soc. Spec. Publ., 406, 81–94, https://doi.org/10.1144/SP406.14, 2015.
- Marrero, S. M., Phillips, F. M., Borchers, B., Lifton, N., Aumer, R., and Balco, G.: Cosmogenic nuclide systematics and the CRONUScalc program, Quat. Geochronol., 31, 160–187, https://doi.org/10.1016/j.quageo.2015.09.005, 2016a.
- Marrero, S. M., Phillips, F. M., Caffee, M. W., and Gosse, J. C.: CRONUS-Earth cosmogenic <sup>36</sup>Cl calibration, Quat. Geochronol., 31, 199–219, https://doi.org/10.1016/j.quageo.2015.10.002, 2016b.
- Matsushi, Y., Sasa, K., Takahashi, T., Sueki, K., Nagashima, Y., and Matsukura, Y.: Denudation rates of carbonate pinnacles in Japanese karst areas, Nucl. Instrum. Meth. B, 268, 1205–1208, https://doi.org/10.1016/j.nimb.2009.10.134, 2010.
- Newson, M. D.: A Model of Subterranean Limestone Erosion in the British Isles Based on Hydrology, T. I. Brit. Geogr., 54, 55, https://doi.org/10.2307/621362, 1971.
- Niemi, N. A., Oskin, M., Burbank, D. W., Heimsath, A. M., and Gabet, E. J.: Effects of bedrock landslides on cosmogenically determined erosion rates, Earth Planet. Sc. Lett., 237, 480–498, https://doi.org/10.1016/j.epsl.2005.07.009, 2005.
- Ott, R. F.: How Lithology Impacts Global Topography, Vegetation, and Animal Biodiversity: A Global-Scale Analysis of Mountainous Regions, Geophys. Res. Lett., 47, e2020GL088649, https://doi.org/10.1029/2020GL088649, 2020.
- Ott, R. F., Gallen, S. F., Caves-Rugenstein, J. K., Ivy-Ochs, S., Helman, D., Fassoulas, C., Vockenhuber, C., Christl, M., and Willett, S. D.: Chemical versus mechanical denudation in meta-clastic and carbonate bedrock catchments on Crete, Greece, and mechanisms for steep and high carbonate topography, J. Geophys. Res.-Earth, 124, 2943–2961, https://doi.org/10.1029/2019JF005142, 2019.
- Ott, R. F., Gallen, S. F., and Granger, D. E.: Cosmogenic nuclide weathering biases: corrections and potential for denudation and weathering rate measurements, Geochronology, 4, 455–470, https://doi.org/10.5194/gchron-4-455-2022, 2022.
- Ouimet, W. B., Whipple, K. X., and Granger, D. E.: Beyond threshold hillslopes: Channel adjustment to base-level fall in tectonically active mountain ranges, Geology, 37, 579–582, https://doi.org/10.1130/G30013A.1, 2009.
- Plan, L.: Factors controlling carbonate dissolution rates quantified in a field test in the Austrian alps, Geomorphology, 68, 201–212, https://doi.org/10.1016/j.geomorph.2004.11.014, 2005.
- Portenga, E. W. and Bierman, P. R.: Understanding Earth's eroding surface with <sup>10</sup>Be, GSA Today, 21, 4–10, https://doi.org/10.1130/G111A.1, 2011.
- Riebe, C. S., Kirchner, J. W., and Granger, D. E.: Quantifying quart enrichment and its consequences for cosmogenic measurements of erosion rates from alluvial sediment and regolith, Geomorphology, 40, 15–19, https://doi.org/10.1016/S0169-555X(01)00031-9, 2001a.
- Riebe, C. S., Kirchner, J. W., Granger, D. E., and Finkel, R. C.: Strong tectonic and weak climatic

- control of long-term chemical weathering rates, Geology, 29, 511–514, https://doi.org/10.1130/0091-7613(2001)029<0511:STAWCC>2.0.CO;2, 2001b.
- Riebe, C. S., Kirchner, J. W., and Finkel, R. C.: Long-term rates of chemical weathering and physical erosion from cosmogenic nuclides and geochemical mass balance, Geochim. Cosmochim. Ac., 67, 4411–4427, https://doi.org/10.1016/S0016-7037(03)00382-X, 2003.
- Riebe, C. S., Kirchner, J. W., and Finkel, R. C.: Erosional and climatic effects on long-term chemical weathering rates in granitic landscapes spanning diverse climate regimes, Earth Planet. Sc. Lett., 224, 547–562, https://doi.org/10.1016/j.epsl.2004.05.019, 2004.
- Rinder, T. and von Hagke, C.: The influence of particle size on the potential of enhanced basalt weathering for carbon dioxide removal Insights from a regional assessment, J. Clean. Prod., 315, 128178, https://doi.org/10.1016/J.JCLEPRO.2021.128178, 2021.
- Royden, L. and Taylor Perron, J.: Solutions of the stream power equation and application to the evolution of river longitudinal profiles, J. Geophys. Res.-Earth, 118, 497–518, https://doi.org/10.1002/jgrf.20031, 2013.
- Ryb, U., Matmon, A., Erel, Y., Haviv, I., Benedetti, L., and Hidy, A. J.: Styles and rates of long-term denuda-tion in carbonate terrains under a Mediterranean to hyper-arid climatic gradient, Earth Planet. Sc. Lett., 406, 142–152, https://doi.org/10.1016/j.epsl.2014.09.008, 2014a.
- Ryb, U., Matmon, A., Erel, Y., Haviv, I., Katz, A., Starinsky, A., Angert, A., and ASTER Team: Controls on denudation rates in tectonically stable Mediterranean carbonate terrain, Geol. Soc. Am. Bull., 126, 553–568, https://doi.org/10.1130/B30886.1, 2014b.
- Ryb, U., Matmon, A., Haviv, I., and Benedetti, L.: Exhumation and uplift coupled with precipitation along the western Dead Sea Rift margin, Geology, 43, 483–486, https://doi.org/10.1130/G36331.1, 2015.
- Schide, K., Gallen, S. F., and Lupker, M.: Modelling the systematics of cosmogenic nuclide signals in fluvial sediments following extreme events, Earth Surf. Proc. Land., 47, 2325–2340, https://doi.org/10.1002/ESP.5381, 2022.
- Schimmelpfennig, I., Benedetti, L., Finkel, R., Pik, R., Blard, P. H., Bourlès, D., Burnard, P., and Williams, A.: Sources of in-situ <sup>36</sup>Cl in basaltic rocks. Implications for calibration of production rates, Quat. Geochronol., 4, 441–461, https://doi.org/10.1016/j.quageo.2009.06.003, 2009.
- Schwanghart, W. and Scherler, D.: Short Communication: Topo-Toolbox 2 – MATLAB-based software for topographic analysis and modeling in Earth surface sciences, Earth Surf. Dynam., 2, 1–7, https://doi.org/10.5194/esurf-2-1-2014, 2014.
- Seybold, H., Berghuijs, W. R., Prancevic, J. P., and Kirchner, J. W.: Global dominance of tectonics over climate in shap-ing river longitudinal profiles, Nat. Geosci., 14, 503–507, https://doi.org/10.1038/s41561-021-00720-5, 2021.
- Simms, M. J.: Tortoises and hares: Dissolution, erosion and isostasy in landscape evolution, Earth Surf. Proc. Land., 29, 477–494, https://doi.org/10.1002/esp.1047, 2004.
- Small, E. E. and Anderson, R. S.: Pleistocene relief production in Laramide mountain ranges, western United

- States, Geology, 26, 123, https://doi.org/10.1130/0091-7613(1998)026<0123:PRPILM>2.3.CO;2, 1998.
- Stallard, R. F. and Edmond, J. M.: Geochemistry of the Amazon, J. Geophys. Res., 86, 9844, https://doi.org/10.1029/JC086iC10p09844, 1981.
- Thomas, F., Godard, V., Bellier, O., Shabanian, E., Ollivier, V., Benedetti, L., Rizza, M., Espurt, N., Guillou, V., Hollender, F., and Molliex, S.: Morphological controls on the dynamics of carbonate landscapes under a mediterranean climate, Terra Nova, 29, 173–182, https://doi.org/10.1111/ter.12260, 2017.
- Thomas, F., Godard, V., Bellier, O., Benedetti, L., Ollivier, V., Rizza, M., Guillou, V., Hollender, F., Aumaître, G., Bourlès, D. L., and Keddadouche, K.: Limited influence of climatic gradients on the denudation of a Mediterranean carbonate landscape, Geomorphology, 316, 44–58, https://doi.org/10.1016/j.geomorph.2018.04.014, 2018.
- von Blanckenburg, F., Hewawasam, T., and Kubik, P. W.: Cosmogenic nuclide evidence for low weathering and denudation in the wet, tropical highlands of Sri Lanka, J. Geophys. Res.-Earth, 109, 3008, https://doi.org/10.1029/2003JF000049, 2004.
- West, A. J., Galy, A., and Bickle, M.: Tectonic and climatic controls on silicate weathering, Earth Planet. Sc. Lett., 235, 211–228, https://doi.org/10.1016/J.EPSL.2005.03.020, 2005.
- White, W. B.: Rate processes: chemical kinetics and karst landform development, in: Groundwater as a geomorphic agent, edited by: La Fleur, R. G., Allen and Unwin, 227–248, ISBN 9781003028833, 1984.
- Whittaker, A. C., Attal, M., Cowie, P. A., Tucker, G. E., and Roberts, G.: Decoding temporal and spatial patterns of fault up-lift using transient river long profiles, Geomorphology, 100, 506–526, https://doi.org/10.1016/J.GEOMORPH.2008.01.018, 2008.
- Williams, P. W. and Dowling, R. K.: Solution of marble in the karst of the Pikikiruna range, Northwest Nelson, New Zealand, Earth Surf. Process., 4, 15–36, https://doi.org/10.1002/ESP.3290040103, 1979.
- Worthington, S. R. H. and Smart, C. C.: Groundwater in karst: conceptual models, in: Encyclopedia of Caves and Karst Science, edited by: Gunn, J., Fitzroy Dearborn, 399–401, ISBN 9780203483855, https://doi.org/10.4324/9780203483855, 2004.
- Xu, S., Liu, C. Q., Freeman, S., Lang, Y. C., Schnabel, C., Tu, C. L., Wilcken, K., and Zhao, Z. Q.: In-situ cosmogenic <sup>36</sup>Cl denudation rates of carbonates in Guizhou karst area, Chinese Sci. Bull., 58, 2473–2479, https://doi.org/10.1007/s11434-013-5756-8, 2013.
- Yang, Y., Lang, Y. C., Xu, S., Liu, C. Q., Cui, L. F., Freeman, S. P. H. T., and Wilcken, K. M.: Combined unsteady denudation and climatic gradient factors constrain carbonate landscape evolution: New insights from in situ cosmogenic <sup>36</sup>Cl, Quat. Geochronol., 58, 101075, https://doi.org/10.1016/J.QUAGEO.2020.101075, 2020.
- Yanites, B. J., Tucker, G. E., and Anderson, R. S.: Numerical and analytical models of cosmogenic radionuclide dynamics in landslide-dominated drainage basins, J. Geophys. Res., 114, 12857, https://doi.org/10.1029/2008JF001088, 2009.
- Zhong, J., Li, S. L., Tao, F., Yue, F., and Liu, C. Q.: Sensitivity of chemical weathering and dissolved carbon dynamics to hydrological conditions in a typical karst river, Sci. Rep.-UK, 71, 1–9, https://doi.org/10.1038/srep42944, 2017.

Supplement of Earth Surf. Dynam., 11, 247–257, 2023 https://doi.org/10.5194/esurf-11-247-2023-supplement © Author(s) 2023. CC BY 4.0 License.





### Supplement of

# Erosion and weathering in carbonate regions reveal climatic and tectonic drivers of carbonate landscape evolution

Richard Ott et al.

Correspondence to: Richard Ott (richard.ott@gfz-potsdam.de)

- esurf-11-247-2023-supplement-title-page.pdf
- Supplement.pdf
- Tab\_S1.xlsx

The copyright of individual parts of the supplement might differ from the article licence.

#### Weathering corrections for denudation rates

Chemical weathering can bias cosmogenic nuclide-derived denudation rates. Regolith weathering can overestimate <sup>36</sup>Cl denudation rates because the soluble target mineral calcite may have a shorter regolith residence time than the bulk rock due to its high solubility. We use the methods proposed by Ott et al. (2022) to correct all alluvial denudation rates for regolith weathering. The correction requires knowledge of the regolith or bedrock composition. In the absence of direct bedrock compositional data, we use the reported bulk chemical composition of the samples as an estimate of regolith composition. We multiply the weight-percent CaO by 1.4 to estimate the calcite fraction in the regolith, take the SiO<sub>2</sub> weight-percent as a fraction quartz, and assign the remainder as other insoluble minerals.

Additionally, we use the mean weathering rates for every area (Israel:  $21 \pm 3$  mm/ka, Crete:  $48 \pm 11$  mm/ka, France:  $37 \pm 8$  mm/ka) for the corrections. On Crete, we estimate 30 cm regolith thickness within the sampled catchments from the European soil database (ESDAC) (Panagos et al., 2012). We use this thickness in conjunction with a density of 1.5 g/cm³ to derive a soil mass of 45 g/cm². The same value is found in southern France, with soil depth estimated from the maps of Chen et al. (2019). For the Soreq catchment in Israel, Ryb et al. (2014b) report regolith thicknesses between 0 and 75 cm. We take the middle (37.5 cm) and use it with the reported regolith density of 1.4 g/cm³ to derive an average soil mass of 52.5 g/cm².

Weathering-corrected denudation rates are similar to conventional denudation rates, with a maximum difference of about 7% (Tab. S2). The sample compositions reported from southern France indicate almost pure limestone. Therefore, the bias for these rocks is minimal. For five samples, the weathering correction could not be applied because the reported nuclide concentration was greater than the theoretical maximum nuclide concentration for the provided parameter combination (N<sub>max</sub>, for definition, see Ott et al., 2022). This is likely linked to uncertainties in the input parameters, such as weathering rate, regolith mass, etc. For some samples considered here, the actual catchment weathering rate is possibly lower than the mean weathering rate for the area. However, the distribution of water sampling stations does not allow deriving weathering rates close to every location sampled for cosmogenic nuclides. In general, the weathering bias in the investigated samples is low due to the low weathering rates and clean limestone composition of many samples. Because the corrections are low and uncertainty exists in some of the correction parameters, we chose to report uncorrected denudation rates in the main text.

Tab. S2: Output of weathering correction calculation for catchment-average denudation rates.

Location	Sample	Denudation rate (mm/ka)	err	Conventional denudation rate (mm/ka)	Rate difference %
Crete	Cl-617-2	87.3	7.0	93.8	6.9
Crete	Cl-617-3				rate could not be calculated because N > Nmax
Crete	Cl-617-6	108.5	5.4	111.9	3.0
Crete	Cl-617-8	159.8	22.5	166.0	3.7
Crete	Cl-617-10	141.5	9.5	146.0	3.0
Crete	Cl-617-15	142.0	13.4	144.7	1.9
Crete	WC-616-8	521.5	117.1	531.8	1.9
France	BRO1B-G	63.0	11.5	62.2	1.1
France	ORM01B-G			37.8	rate could not be calculated because N > Nmax
France	ORM02B-G	72.6	23.4	72.0	0.8
France	ORM02B-S	81.7	21.7	80.9	0.9
France	ORM03B-G	67.1	23.3	66.5	1.0
France	ORM03B-S	67.9	20.5	67.2	1.0
France	PLBS-1G	56.4	8.0	56.1	0.4
France	PLBS-1S			48.9	rate could not be calculated because N > Nmax
France	PLBS-2S	53.9	7.3	53.7	0.3
France	PLBS-3G	100.7	19.8	100.6	0.1
France	PLBS-4G	84.4	14.7	84.1	0.4
France	PLS-E1	67.4	19.3	67.2	0.3
France	PLS-E2	75.1	22.1	74.9	0.2
France	REC01B-S	98.3	28.1	97.9	0.4
France	REC02B-G	93.3	28.1	93.1	0.3
France	REC02B-S	101.8	35.0	101.4	0.4
France	ROQ01B-G	59.7	11.3	59.1	1.0
France	ROQ01B-S	70.8	12.8	70.4	0.6
France	TAP01B-G	60.0	19.6	59.5	0.9
France	TAP01B-S	74.1	21.0	73.6	0.6
France	TAP02B-G	53.5	17.4	53.0	1.0
France	TAP02B-S	56.6	17.9	56.2	0.8
France	VID01B-S	64.7	10.6	64.3	0.7
France	VID02B-S	82.5	15.3	82.1	0.5
Israel/Soreq	SQSED1			41.5	rate could not be calculated because N > Nmax
Israel/Soreq	SQSED2	60.8	1.4	63.4	4.1
Israel/Soreq	SQSED3	59.6	1.3	61.1	2.5
Israel/Soreq	SQSED4	117.3	5.3	118.7	1.1
Israel/Soreq	SQSED5	50.5	0.4	53.1	4.9

Israel/Soreq	SQSED6	58.6	1.2	59.9	2.1
Israel/Soreq	SQSED7			49.8	rate could not be calculated because N > Nmax

Tab S3: Raw and precipitation corrected water data from southern France.  $[Ca^{2+}]$  and  $[Mg^{2+}]$ . n- number of samples, min - minimum concentration, max - maximum concentration measured.

National Code of station	Area	Lon (°)	Lat (°)			Ca (m	g/I)			Mg	(mg/l)			c	l (mg/l)	
				n		4	min		65.6	average	correct	3 5	0.0	min	max	average
09678X0109/HY	Luberon	5.3802	43.8203	1	3.3016	3		87.0	87.0	91.8 80.9	ed			3.4	3.4	3.4
09685X0011/F	Luberon	5.4057	43.8285	5	5.7099		max	62.0	62.0	106.2 87.2		7	77.7	6.5	8.7	7.6
09681X0069/FO	Luberon	5.4622	43.8399	2		4	91.8	56.6	65.0	86.2 70.7	<b>n</b> 91.7	0 /	-7.0	3.4	3.5	3.5
09685X0013/F	Luberon	5.4171	43.7862	3	3.2898	9		56.1	56.1	112.7		8 6	57.0	1.3	1.5	1.4
09685X0012/HY	Luberon	5.4226	43.7868	3	5.6600	43.	91.8	57.2	64.0	103.4	1 80.8	8 88.6	3	4.9	6.3	5.8
09674X0089/F	Luberon	5.3852	43.8361	3	2911	14	77.0	49.0	51.9	50.8 59.4		131.7	1	2.6	3.5	3.0
09686X0019/F	Luberon	5.5380	43.7930	31				73.0	85.0	63.9 87.0	5 106.0	118.8	1	7.0	9.5	8.1
09676X0053/P	Luberon	5.1791	43.7531	7			85.2	64.5	70.4	62.0		122.3	7	4.4	16.1	13.5
09175X0016/HY	Lure	5.7888	44.1090				102.4	60.6	139.6	61.1 56.1	2 87.1	89.5		0.5	0.5	0.5
09431X0010/HY	Lure		3 5.83	374				132.0	132.0	59.5 50.0				0.5	1.5	1.0
09176X0008/TX	Lure		44.0668 5 5.89	244			110.0	119.0	119.0	77.8 67.0	3 86.2	2 92.9	3	9.2	10.8	9.9
09431X0013/HY	Lure		44.1311	744			80.0	116.0	129.0	89.1		69.8		1.9	1.9	1.9
09424X0015/HY	Lure		3 5.78	359				61.4	118.0	132.0	3 70.4	9		1.5	1.5	1.5
09153X1005/HY	Ventoux		44.0506				93.5	85.3	108.0	119.0		9 72.0		3.7	4.1	3.8
09153X1004/HY	Ventoux		1 5.70	59			82.8	66.8	73.4	122.5	3 112.6	72.0	1	8.6	8.6	8.6
09154X1004/SO	Ventoux		44.0956					60.4	78.8	89.7 93.2		4		1.9	2.3	2.2
09157X0014/HY	Ventoux		1 5.28 44.1881	395			88.9			70.0	31			1.2	1.4	1.3
09165X1006/HY	Ventoux		4 5.27	 734			68.0			72.2	102.9			5.1	7.5	6.2
09156X0074/F	Ventoux		44.2056											1.4	2.1	1.7
10212X0020/HY	Sainte Victoire		1 5.33	148			74.0				7 50.8			5.5	27.6	13.2
10213X0051/P	Sainte Victoire		44.1923				104.0				3 59.3			31.8	31.8	31.8
10213X0050/HY	Sainte Victoire		3 5.22	233							3 33.3			18.4	18.4	18.4
10213X0121/HY	Sainte Victoire		44.1895 7 5.43	120			123.0				5 63.8			6.7	10.4	9.2
10451X0041/F	Sainte Baume		7 5.42 44.1248	139			55.0							20.8	63.5	42.2
10444X0028/F	Sainte Baume		8 5.20	) 71							3 86.9			44.2	54.9	50.4
10444X0026/DA	Sainte Baume		44.1833				120.0				1 62 0			27.5	31.0	28.9
10443X0291/HY	Sainte Baume		8 5.57	52			49.0				1 62.0			17.2	21.9	19.0
			43.5188	3							1 61.0					
		5.6411	43.5285	1			53.5									
		5.6422	43.5232				46.0				4 56.1					
		5.6013	43.5563	7			CF									
		5.7711	43.3098				65.5				1 59.5					
			2 5.75	559			61.0									

corrected	<b>n</b> 3.1	min	max	average 5.1
	1 7.3	5.1	5.1 3.7	4.5 10.8 6.3 1.0 14.3
	10		4.8	5.1
2.7	2 1.0	10.1	11.4	25.7 2.3 3.3 4.1 4.3
	3 5.7	6.1	6.5 0.8	2.1
	3 2.1		1.4	2.7 1.2 2.3 2.3 3.3 2.2
	3 7.8	13.9	14.9	21.1 15.6 9.9 7.9 10.9
	31	4.1	8.0	15.6 10.6
11.8	8 0.3	10.7	31.0	8.7
	18	0.8	9.2 2.3	
0.8	2 4		9.2 2.5	
9.6	4		6.1 3.8	
1.6	6		5.1 1.0	
1.4	5		3.1	
3.6	4	2.4		
8.5	1	2.4	3.1 1.2	
2.0	3		1.2 2.1	
1.2	7		2.5 2.0	
6.0	8		2.4 2.8	
1.5	9		3.9 1.9	
11.8	3		2.4	
30.8	1	17.0	27.9	
17.7	1 8.7	15.6	15.6	
	7	9.9	9.9 6.2	
41.4	3	9.9		
49.3	3		9.0 7.5	
28.2	9		17.2	
18.4	1 4	11.3	22.0	
		9.7	12.0	
		7.6	10.2	

Tab. S4: Weathering rates calculated using estimated recharge areas from topography (Fig. S1) together with average P and AET values for the entire mountain range of the sampled spring, well or river.

						Estimated recharge areas		Mountain range average		e averages	
Location	Country	N (°)	E (°)	[Ca <sup>2+</sup> ] (mg/l)	[Mg <sup>2+</sup> ] (mg/l)	P (mm/a)	AET (mm/a)	Dissolution rate (mm/a)	P (mm/a)	AET (mm/a)	Dissolution rate (mm/a)
Agur1	Israel	31.7207	34.9162	61	35				490	291	0.021 ± 0.005
Agur2	Israel	31.7241	34.9139	56	35				490	291	0.02 ± 0.004
Agur3	Israel	31.7074	34.9399	59	33				490	291	0.02 ± 0.004
Agur4	Israel	31.6842	34.9803	62	32				490	291	0.02 ± 0.004
Agur5	Israel	31.6796	34.9890	91	34				490	291	0.026 ± 0.006
Agur6	Israel	31.6796	35.0088	58	29				490	291	0.019 ± 0.004
Agur7	Israel	31.6789	35.0276	57	29				490	291	0.018 ± 0.004
Agur8	Israel	31.7116	35.0106	70	30				490	291	0.021 ± 0.005
EnKarem1	Israel	31.7795	35.1557	48	14				490	291	0.013 ± 0.003
EnKarem13	Israel	31.7434	35.1531	53	24				490	291	0.016 ± 0.004
EnKarem14	Israel	31.7986	35.1697	61	27				490	291	0.019 ± 0.004
EnKarem15	Israel	31.7877	35.1622	65	30				490	291	0.02 ± 0.005
EnKarem16	Israel	31.7447	35.1762	60	25				490	291	0.018 ± 0.004
EnKarem17	Israel	31.7422	35.1643	36	21				490	291	0.012 ± 0.003
EnKarem3	Israel	31.8002	35.1251	62	33				490	291	0.02 ± 0.005
EnKarem9	Israel	31.8052	35.1716	55	24				490	291	0.017 ± 0.004
Karem9+1	Israel	31.8052	35.1716	61	26				490	291	0.018 ± 0.004
Eshtaol1	Israel	31.7769	35.0103	68	37				490	291	0.022 ± 0.005
Eshtaol2a	Israel	31.7770	35.0126	66	39				490	291	0.023 ± 0.005
Eshtaol3	Israel	31.8155	35.0232	74	35				490	291	0.023 ± 0.005
Eshtaol4	Israel	31.7995	35.0120	85	38				490	291	0.026 ± 0.006
Eshtaol5	Israel	31.7772	35.0255	59	31				490	291	0.019 ± 0.004
Eshtaol6	Israel	31.8097	35.0151	85	37				490	291	0.026 ± 0.006
Eshtaol7	Israel	31.7681	35.0122	52	29				490	291	0.017 ± 0.004
Eshtaol8	Israel	31.8028	35.0189	65	29				490	291	0.02 ± 0.004
Eshtaol9	Israel	31.7892	35.0161	69	31				490	291	0.021 ± 0.005
Hartuv3	Israel	31.7605	35.0085	61	37				490	291	0.021 ± 0.005
Hartuv4	Israel	31.7505	35.0001	68	35				490	291	0.022 ± 0.005
Modieen1	Israel	31.8605	35.0330	80	40				490	291	0.026 ± 0.006
Modieen2	Israel	31.8505	35.0435	81	30				490	291	0.023 ± 0.005
Modieen3	Israel	31.8266	35.0307	66	29				490	291	0.02 ± 0.004
Modieen4	Israel	31.8402	35.0361	60	27				490	291	0.018 ± 0.004
Uriya2	Israel	31.7958	34.9491	58	36				490	291	0.02 ± 0.005
Uriya3	Israel	31.8005	34.9576	66	39				490	291	0.023 ± 0.005
Uriya4	Israel	31.8159	34.9178	76	44				490	291	0.026 ± 0.006
Uriya6	Israel	31.8016	34.9508	80	37				490	291	0.025 ± 0.006
Uriya7	Israel	31.7621	34.9643	77	37				490	291	0.024 ± 0.005
Uriya8	Israel	31.8252	34.9428	88	40				490	291	0.027 ± 0.006
Uriya9a	Israel	31.7950	34.9754	78	38				490	291	0.025 ± 0.006
09678X0109/HY	France	43.8203	5.3802	91.7	3.1	794	424	0.035 ± 0.008	773	433	0.032 ± 0.007
09685X0011/F	France	43.8285	5.4057	80.8	7.3	802	443	0.032 ± 0.007	773	433	0.03 ± 0.007
09681X0069/FO	France	43.8399	5.4622	106.0	2.7	833	337	0.054 ± 0.012	773	433	0.037 ± 0.008

09685X0013/FF   France   43.7862   5.4171   87.1   1.0   806   697   0.011±0.002   773   433   0.031±0.007     09685X0013/FF   France   43.7868   5.4266   862   5.7   82.3   701   0.011±0.003   773   433   0.032±0.007     09676X0059/F   France   43.7930   5.5380   112.6   7.8   793   418   0.046±0.006   773   433   0.025±0.006     09686X0019/F   France   43.7531   5.1791   102.9   11.8   707   484   0.026±0.006   725   445   0.033±0.007     09175X0016/FFF   France   44.1090   5.7888   50.8   0.3   1081   647   0.022±0.005   923   500   0.022±0.005     09431X0010/FFF   France   44.0668   5.8374   59.3   0.8   962   644   0.019±0.004   923   500   0.022±0.005     09431X0013/FFF   France   44.0566   5.7859   86.9   1.6   975   613   0.032±0.007   923   500   0.032±0.007     09431X0013/FFFF   France   44.0956   5.7059   62.0   1.4   1004   586   0.027±0.006   923   500   0.027±0.006     09153X1005/FFFFFFFFFFFFFFFFFFFFFFFFFFFFFFFFFFF												
09674X0089/F	09685X0013/F	France	43.7862	5.4171	87.1	1.0	806	697	0.01 ± 0.002	773	433	0.03 ± 0.007
09686X0019/F	09685X0012/HY	France	43.7868	5.4226	86.2	5.7	823	701	0.011 ± 0.003	773	433	0.032 ± 0.007
09676X0053/P	09674X0089/F	France	43.8361	5.3852	70.4	2.1	761	398	0.026 ± 0.006	773	433	0.025 ± 0.006
O9175X0016/HY   France   44.1090   5.7888   50.8   0.3   1081   647   0.022±0.005   923   500   0.022±0.005	09686X0019/F	France	43.7930	5.5380	112.6	7.8	793	418	0.046 ± 0.01	773	433	0.041 ± 0.009
09431X0010/HY   France	09676X0053/P	France	43.7531	5.1791	102.9	11.8	707	484	0.026 ± 0.006	725	445	0.033 ± 0.007
09176X0008/TX	09175X0016/HY	France	44.1090	5.7888	50.8	0.3	1081	647	0.022 ± 0.005	923	500	0.022 ± 0.005
09431X0013/HY         France         44.0506         5.7859         86.9         1.6         975         613         0.032±0.007         923         500         0.038±0.008           09424X0015/HY         France         44.0956         5.7059         62.0         1.4         1004         586         0.027±0.006         923         500         0.027±0.006           09153X1005/HY         France         44.1881         5.2895         61.0         3.6         1046         399         0.042±0.009         912         444         0.031±0.007           09153X1004/HY         France         44.2056         5.2734         56.1         8.5         999         345         0.043±0.01         912         444         0.031±0.007           09154X1004/SO         France         44.1923         5.3148         59.5         2.0         942         342         0.037±0.008         912         444         0.024±0.005           09157X0014/HY         France         44.1895         5.2233         50.0         1.2         963         259         0.036±0.008         912         444         0.04±0.009           09156X0704/F         France         44.1833         5.2071         67.0         1.5         891         394	09431X0010/HY	France	44.0668	5.8374	59.3	0.8	962	644	0.019 ± 0.004	923	500	0.025 ± 0.006
09424X0015/HY         France         44.0956         5.7059         62.0         1.4         1004         586         0.027 ± 0.006         923         500         0.027 ± 0.006           09153X1005/HY         France         44.1881         5.2895         61.0         3.6         1046         399         0.042 ± 0.009         912         444         0.031 ± 0.007           09153X1004/HY         France         44.2056         5.2734         56.1         8.5         999         345         0.043 ± 0.01         912         444         0.031 ± 0.007           09154X1004/SO         France         44.1923         5.3148         59.5         2.0         942         342         0.037 ± 0.008         912         444         0.029 ± 0.006           09157X0014/HY         France         44.1895         5.2233         50.0         1.2         963         259         0.036 ± 0.008         912         444         0.024 ± 0.005           09155X0074/F         France         44.1833         5.2071         67.0         1.5         891         394         0.034 ± 0.008         912         444         0.032 ± 0.007           10213X0050/HY         France         43.5188         5.5752         88.6         11.8         744	09176X0008/TX	France	44.1311	5.8944	63.8	9.6	894	184	0.054 ± 0.012	923	500	0.032 ± 0.007
O9153X1005/HY   France	09431X0013/HY	France	44.0506	5.7859	86.9	1.6	975	613	0.032 ± 0.007	923	500	0.038 ± 0.008
O9153X1004/HY   France	09424X0015/HY	France	44.0956	5.7059	62.0	1.4	1004	586	0.027 ± 0.006	923	500	0.027 ± 0.006
09154X1004/SO         France         44.1923         5.3148         59.5         2.0         942         342         0.037±0.008         912         444         0.029±0.006           09157X0014/HY         France         44.1895         5.2233         50.0         1.2         963         259         0.036±0.008         912         444         0.024±0.005           09165X1006/HY         France         44.1248         5.4139         77.7         6.0         904         493         0.035±0.008         912         444         0.04±0.009           09156X0074/F         France         44.1833         5.2071         67.0         1.5         891         394         0.034±0.008         912         444         0.032±0.007           10212X0020/HY         France         43.5188         5.5752         88.6         11.8         744         378         0.038±0.008         738         366         0.038±0.009           10213X0050/HY         France         43.5232         5.6422         118.8         17.7         735         381         0.05±0.011         738         366         0.052±0.012           10213X0121/HY         France         43.5563         5.6013         122.3         8.7         758         340 <td>09153X1005/HY</td> <td>France</td> <td>44.1881</td> <td>5.2895</td> <td>61.0</td> <td>3.6</td> <td>1046</td> <td>399</td> <td>0.042 ± 0.009</td> <td>912</td> <td>444</td> <td>0.031 ± 0.007</td>	09153X1005/HY	France	44.1881	5.2895	61.0	3.6	1046	399	0.042 ± 0.009	912	444	0.031 ± 0.007
09157X0014/HY         France         44.1895         5.2233         50.0         1.2         963         259         0.036±0.008         912         444         0.024±0.005           09165X1006/HY         France         44.1248         5.4139         77.7         6.0         904         493         0.035±0.008         912         444         0.04±0.009           09156X0074/F         France         44.1833         5.2071         67.0         1.5         891         394         0.034±0.008         912         444         0.032±0.007           10212X0020/HY         France         43.5188         5.5752         88.6         11.8         744         378         0.038±0.008         738         366         0.038±0.009           10213X0050/HY         France         43.5285         5.6411         131.7         30.8         776         336         0.074±0.017         738         366         0.063±0.014           10213X0121/HY         France         43.5563         5.6013         122.3         8.7         758         340         0.055±0.012         738         366         0.049±0.011           10451X0041/F         France         43.3016         5.7559         92.9         49.3         790         439 </td <td>09153X1004/HY</td> <td>France</td> <td>44.2056</td> <td>5.2734</td> <td>56.1</td> <td>8.5</td> <td>999</td> <td>345</td> <td>0.043 ± 0.01</td> <td>912</td> <td>444</td> <td>0.031 ± 0.007</td>	09153X1004/HY	France	44.2056	5.2734	56.1	8.5	999	345	0.043 ± 0.01	912	444	0.031 ± 0.007
09165X1006/HY         France         44.1248         5.4139         77.7         6.0         904         493         0.035±0.008         912         444         0.04±0.009           09156X0074/F         France         44.1833         5.2071         67.0         1.5         891         394         0.034±0.008         912         444         0.032±0.007           10212X0020/HY         France         43.5188         5.5752         88.6         11.8         744         378         0.038±0.008         738         366         0.038±0.009           10213X0051/P         France         43.5285         5.6411         131.7         30.8         776         336         0.074±0.017         738         366         0.063±0.014           10213X0050/HY         France         43.5232         5.6422         118.8         17.7         735         381         0.05±0.011         738         366         0.052±0.012           10213X0121/HY         France         43.5963         5.6013         122.3         8.7         758         340         0.055±0.012         738         366         0.049±0.011           10445X0024/F         France         43.3098         5.7711         89.5         41.4         794         464 </td <td>09154X1004/SO</td> <td>France</td> <td>44.1923</td> <td>5.3148</td> <td>59.5</td> <td>2.0</td> <td>942</td> <td>342</td> <td>0.037 ± 0.008</td> <td>912</td> <td>444</td> <td>0.029 ± 0.006</td>	09154X1004/SO	France	44.1923	5.3148	59.5	2.0	942	342	0.037 ± 0.008	912	444	0.029 ± 0.006
09156X0074/F         France         44.1833         5.2071         67.0         1.5         891         394         0.034 ± 0.008         912         444         0.032 ± 0.007           10212X0020/HY         France         43.5188         5.5752         88.6         11.8         744         378         0.038 ± 0.008         738         366         0.038 ± 0.009           10213X0051/P         France         43.5285         5.6411         131.7         30.8         776         336         0.074 ± 0.017         738         366         0.063 ± 0.014           10213X0050/HY         France         43.5232         5.6422         118.8         17.7         735         381         0.05 ± 0.011         738         366         0.052 ± 0.012           10213X0121/HY         France         43.5563         5.6013         122.3         8.7         758         340         0.055 ± 0.012         738         366         0.049 ± 0.011           10451X0041/F         France         43.3016         5.7559         92.9         49.3         790         439         0.054 ± 0.012         773         423         0.049 ± 0.011           10444X0028/F         France         43.2898         5.7099         69.8         28.2         7	09157X0014/HY	France	44.1895	5.2233	50.0	1.2	963	259	0.036 ± 0.008	912	444	0.024 ± 0.005
10212X0020/HY         France         43.5188         5.5752         88.6         11.8         744         378         0.038 ± 0.008         738         366         0.038 ± 0.009           10213X0051/P         France         43.5285         5.6411         131.7         30.8         776         336         0.074 ± 0.017         738         366         0.063 ± 0.014           10213X0050/HY         France         43.5232         5.6422         118.8         17.7         735         381         0.05 ± 0.011         738         366         0.052 ± 0.012           10213X0121/HY         France         43.5563         5.6013         122.3         8.7         758         340         0.055 ± 0.012         738         366         0.049 ± 0.011           10451X0041/F         France         43.3098         5.7711         89.5         41.4         794         464         0.046 ± 0.01         773         423         0.049 ± 0.011           10444X0028/F         France         43.3016         5.7559         92.9         49.3         790         439         0.054 ± 0.012         773         423         0.035 ± 0.012           10444X0026/DA         France         43.2898         5.7099         69.8         28.2	09165X1006/HY	France	44.1248	5.4139	77.7	6.0	904	493	0.035 ± 0.008	912	444	0.04 ± 0.009
10213X0051/P         France         43.5285         5.6411         131.7         30.8         776         336         0.074 ± 0.017         738         366         0.063 ± 0.014           10213X0050/HY         France         43.5232         5.6422         118.8         17.7         735         381         0.05 ± 0.011         738         366         0.052 ± 0.012           10213X0121/HY         France         43.5563         5.6013         122.3         8.7         758         340         0.055 ± 0.012         738         366         0.049 ± 0.011           10451X0041/F         France         43.3098         5.7711         89.5         41.4         794         464         0.046 ± 0.01         773         423         0.049 ± 0.011           10444X0028/F         France         43.3016         5.7559         92.9         49.3         790         439         0.054 ± 0.012         773         423         0.035 ± 0.012           10444X0026/DA         France         43.2898         5.7099         69.8         28.2         795         516         0.029 ± 0.006         773         423         0.036 ± 0.008           10443X0291/HY         France         43.2911         5.6600         72.0         18.4	09156X0074/F	France	44.1833	5.2071	67.0	1.5	891	394	0.034 ± 0.008	912	444	0.032 ± 0.007
10213X0050/HY         France         43.5232         5.6422         118.8         17.7         735         381         0.05±0.011         738         366         0.052±0.012           10213X0121/HY         France         43.5563         5.6013         122.3         8.7         758         340         0.055±0.012         738         366         0.049±0.011           10451X0041/F         France         43.3098         5.7711         89.5         41.4         794         464         0.046±0.01         773         423         0.049±0.011           10444X0028/F         France         43.3016         5.7559         92.9         49.3         790         439         0.054±0.012         773         423         0.053±0.012           10444X0026/DA         France         43.2898         5.7099         69.8         28.2         795         516         0.029±0.006         773         423         0.036±0.008           10443X0291/HY         France         43.2911         5.6600         72.0         18.4         748         488         0.025±0.005         773         423         0.033±0.007           Kournas Lake         Greece         35.3310         24.2801         118.8         40.9         908         35	10212X0020/HY	France	43.5188	5.5752	88.6	11.8	744	378	0.038 ± 0.008	738	366	0.038 ± 0.009
10213X0121/HY         France         43.5563         5.6013         122.3         8.7         758         340         0.055 ± 0.012         738         366         0.049 ± 0.011           10451X0041/F         France         43.3098         5.7711         89.5         41.4         794         464         0.046 ± 0.01         773         423         0.049 ± 0.011           10444X0028/F         France         43.3016         5.7559         92.9         49.3         790         439         0.054 ± 0.012         773         423         0.053 ± 0.012           10444X0026/DA         France         43.2898         5.7099         69.8         28.2         795         516         0.029 ± 0.006         773         423         0.036 ± 0.008           10443X0291/HY         France         43.2911         5.6600         72.0         18.4         748         488         0.025 ± 0.005         773         423         0.033 ± 0.007           Kournas Lake         Greece         35.3310         24.2801         118.8         40.9         908         355         0.093 ± 0.021         900         287         0.103 ± 0.023           Vrysses         Greece         35.1396         24.5288         155.3         39.7         984	10213X0051/P	France	43.5285	5.6411	131.7	30.8	776	336	0.074 ± 0.017	738	366	0.063 ± 0.014
10451X0041/F         France         43.3098         5.7711         89.5         41.4         794         464         0.046 ± 0.01         773         423         0.049 ± 0.011           10444X0028/F         France         43.3016         5.7559         92.9         49.3         790         439         0.054 ± 0.012         773         423         0.053 ± 0.012           10444X0026/DA         France         43.2898         5.7099         69.8         28.2         795         516         0.029 ± 0.006         773         423         0.036 ± 0.008           10443X0291/HY         France         43.2911         5.6600         72.0         18.4         748         488         0.025 ± 0.005         773         423         0.033 ± 0.007           Kournas Lake         Greece         35.3310         24.2801         118.8         40.9         908         355         0.093 ± 0.021         900         287         0.103 ± 0.023           Vrysses         Greece         35.3764         24.2010         62.8         9.2         892         345         0.04 ± 0.009         900         287         0.045 ± 0.01           Agia Fotini         Greece         35.1396         24.5288         155.3         39.7         984 <td>10213X0050/HY</td> <td>France</td> <td>43.5232</td> <td>5.6422</td> <td>118.8</td> <td>17.7</td> <td>735</td> <td>381</td> <td>0.05 ± 0.011</td> <td>738</td> <td>366</td> <td>0.052 ± 0.012</td>	10213X0050/HY	France	43.5232	5.6422	118.8	17.7	735	381	0.05 ± 0.011	738	366	0.052 ± 0.012
10444X0028/F         France         43.3016         5.7559         92.9         49.3         790         439         0.054 ± 0.012         773         423         0.053 ± 0.012           10444X0026/DA         France         43.2898         5.7099         69.8         28.2         795         516         0.029 ± 0.006         773         423         0.036 ± 0.008           10443X0291/HY         France         43.2911         5.6600         72.0         18.4         748         488         0.025 ± 0.005         773         423         0.033 ± 0.007           Kournas Lake         Greece         35.3310         24.2801         118.8         40.9         908         355         0.093 ± 0.021         900         287         0.103 ± 0.023           Vrysses         Greece         35.3764         24.2010         62.8         9.2         892         345         0.04 ± 0.009         900         287         0.045 ± 0.01           Agia Fotini         Greece         35.1396         24.5288         155.3         39.7         984         248         0.15 ± 0.033         962         397         0.115 ± 0.026           Preveli         Greece         35.1635         24.4742         86.7         24.5 <td< td=""><td>10213X0121/HY</td><td>France</td><td>43.5563</td><td>5.6013</td><td>122.3</td><td>8.7</td><td>758</td><td>340</td><td>0.055 ± 0.012</td><td>738</td><td>366</td><td>0.049 ± 0.011</td></td<>	10213X0121/HY	France	43.5563	5.6013	122.3	8.7	758	340	0.055 ± 0.012	738	366	0.049 ± 0.011
10444X0026/DA         France         43.2898         5.7099         69.8         28.2         795         516         0.029 ± 0.006         773         423         0.036 ± 0.008           10443X0291/HY         France         43.2911         5.6600         72.0         18.4         748         488         0.025 ± 0.005         773         423         0.033 ± 0.007           Kournas Lake         Greece         35.3310         24.2801         118.8         40.9         908         355         0.093 ± 0.021         900         287         0.103 ± 0.023           Vrysses         Greece         35.3764         24.2010         62.8         9.2         892         345         0.04 ± 0.009         900         287         0.045 ± 0.01           Agia Fotini         Greece         35.1396         24.5288         155.3         39.7         984         248         0.15 ± 0.033         962         397         0.115 ± 0.026           Preveli         Greece         35.1635         24.4742         86.7         24.5         940         460         0.056 ± 0.012         962         397         0.066 ± 0.015	10451X0041/F	France	43.3098	5.7711	89.5	41.4	794	464	0.046 ± 0.01	773	423	0.049 ± 0.011
10443X0291/HY         France         43.2911         5.6600         72.0         18.4         748         488         0.025 ± 0.005         773         423         0.033 ± 0.007           Kournas Lake         Greece         35.3310         24.2801         118.8         40.9         908         355         0.093 ± 0.021         900         287         0.103 ± 0.023           Vrysses         Greece         35.3764         24.2010         62.8         9.2         892         345         0.04 ± 0.009         900         287         0.045 ± 0.01           Agia Fotini         Greece         35.1396         24.5288         155.3         39.7         984         248         0.15 ± 0.033         962         397         0.115 ± 0.026           Preveli         Greece         35.1635         24.4742         86.7         24.5         940         460         0.056 ± 0.012         962         397         0.066 ± 0.015	10444X0028/F	France	43.3016	5.7559	92.9	49.3	790	439	0.054 ± 0.012	773	423	0.053 ± 0.012
Kournas Lake         Greece         35.3310         24.2801         118.8         40.9         908         355         0.093 ± 0.021         900         287         0.103 ± 0.023           Vrysses         Greece         35.3764         24.2010         62.8         9.2         892         345         0.04 ± 0.009         900         287         0.045 ± 0.01           Agia Fotini         Greece         35.1396         24.5288         155.3         39.7         984         248         0.15 ± 0.033         962         397         0.115 ± 0.026           Preveli         Greece         35.1635         24.4742         86.7         24.5         940         460         0.056 ± 0.012         962         397         0.066 ± 0.015	10444X0026/DA	France	43.2898	5.7099	69.8	28.2	795	516	0.029 ± 0.006	773	423	0.036 ± 0.008
Vrysses         Greece         35.3764         24.2010         62.8         9.2         892         345         0.04 ± 0.009         900         287         0.045 ± 0.01           Agia Fotini         Greece         35.1396         24.5288         155.3         39.7         984         248         0.15 ± 0.033         962         397         0.115 ± 0.026           Preveli         Greece         35.1635         24.4742         86.7         24.5         940         460         0.056 ± 0.012         962         397         0.066 ± 0.015	10443X0291/HY	France	43.2911	5.6600	72.0	18.4	748	488	0.025 ± 0.005	773	423	0.033 ± 0.007
Vrysses         Greece         35.3764         24.2010         62.8         9.2         892         345         0.04 ± 0.009         900         287         0.045 ± 0.01           Agia Fotini         Greece         35.1396         24.5288         155.3         39.7         984         248         0.15 ± 0.033         962         397         0.115 ± 0.026           Preveli         Greece         35.1635         24.4742         86.7         24.5         940         460         0.056 ± 0.012         962         397         0.066 ± 0.015	Kournas Lake	Greece	35.3310	24.2801	118.8	40.9	908	355	0.093 ± 0.021	900	287	0.103 ± 0.023
Preveli Greece 35.1635 24.4742 86.7 24.5 940 460 0.056 ± 0.012 962 397 0.066 ± 0.015	Vrysses		35.3764	24.2010	62.8	9.2	892	345	0.04 ± 0.009	900	287	0.045 ± 0.01
Plaking -	Agia Fotini	Greece	35.1396	24.5288	155.3	39.7	984	248	0.15 ± 0.033	962	397	0.115 ± 0.026
District -	Preveli	Greece	35.1635	24.4742	86.7	24.5	940	460	0.056 ± 0.012	962	397	0.066 ± 0.015
	Plakias	Greece	35.1930	24.3948	64.0	16.7	917	370	0.046 ± 0.01	962	397	0.048 ± 0.011
Lyttos Greece 35.2279 25.3620 45.5 8.4 877 350 0.029 ± 0.007 799 347 0.025 ± 0.006	Lyttos	Greece										
Samaria Greece 35.4371 24.1267 29.4 14.6 876 315 0.026±0.006 900 287 0.029±0.006	Samaria	Greece										
Selena Greece 35.2905 25.5310 29.8 10.8 847 292 0.024 ± 0.005 799 347 0.019 ± 0.004	Selena	Greece										
Lentas Greece 34.9518 24.9276 51.7 30.0 847 226 0.055 ± 0.012 770 215 0.049 ± 0.011												
Rouvas Greece 35.1381 24.9606 19.7 13.0 1011 263 0.027 ± 0.006 900 287 0.022 ± 0.005												
Stylos Greece 35.4353 24.1274 23.6 12.0 876 315 0.021 ± 0.005 900 287 0.023 ± 0.005												
Kiliaris River Greece 35.4604 24.1551 39.8 5.3 785 435 0.016 ± 0.004 900 287 0.028 ± 0.006	· ·											
Zaros Greece 35.1415 24.9065 28.0 14.0 1013 257 0.034 ± 0.008 988 282 0.032 ± 0.007												
Aposelemis Greece 35.3298 25.3333 112.4 23.9 795 415 0.054±0.012 799 347 0.064±0.014												
Kourna Lake Greece 35.3304 24.2753 101.6 43.3 908 355 0.085 ± 0.019 900 287 0.094 ± 0.021												
Kourtaliotis Greece 35.1548 24.4730 72.3 24.9 940 460 0.049 ± 0.011 962 397 0.058 ± 0.013												

Tab. S5: Pearson'r and p values for the correlation of topographic and climatic variables from catchments with alluvial samples.

Pearson's r	Denudation	Mean elevation	Mean precipitation	Mean AET	Mean runoff	Mean local relief	Mean slope
Denudation	1.000	0.470	0.684	0.357	0.387	0.652	0.503
Mean elevation	0.470	1.000	0.249	-0.335	0.631	0.338	0.024
Mean precipitation	0.684	0.249	1.000	0.577	0.509	0.773	0.797
Mean AET	0.357	-0.335	0.577	1.000	-0.409	0.372	0.648
Mean runoff	0.387	0.631	0.509	-0.409	1.000	0.473	0.207
Mean local relief	0.652	0.338	0.773	0.372	0.473	1.000	0.872
Mean slope	0.503	-0.024	0.797	0.648	0.207	0.872	1.000
n-values	Denudation	Mean	Mean	Mean	Mean	Mean local	Mean
p-values	Denudation	Mean elevation	Mean precipitation	Mean AET	Mean runoff	Mean local relief	Mean slope
p-values  Denudation	Denudation 1.000						
		elevation	precipitation	AET	runoff	relief	slope
Denudation	1.000	elevation 0.002	precipitation 0.000	AET 0.020	runoff 0.011	relief 0.000	slope 0.001
Denudation Mean elevation	1.000 0.002	elevation 0.002 1.000	0.000 0.112	AET 0.020 0.030	runoff 0.011 0.000	relief 0.000 0.029	slope 0.001 0.879
Denudation Mean elevation Mean precipitation	1.000 0.002 0.000	0.002 1.000 0.112	0.000 0.112 1.000	AET 0.020 0.030 0.000	runoff 0.011 0.000 0.001	relief 0.000 0.029 0.000	0.001 0.879 0.000
Denudation Mean elevation Mean precipitation Mean AET	1.000 0.002 0.000 0.020	elevation 0.002 1.000 0.112 0.030	0.000 0.112 1.000 0.000	AET 0.020 0.030 0.000 1.000	runoff 0.011 0.000 0.001 0.007	relief 0.000 0.029 0.000 0.015	slope 0.001 0.879 0.000 0.000

Tab. S6: Pearson's r and p values for the correlation of topographic and climatic variables from catchments with weathering rates.

Pearson's r	Weathering rate	Mean slope	Mean local relief	Mean precipitation	Mean runoff
Weathering rate	1.000	0.382	0.517	0.522	0.503
Mean slope	0.382	1.000	0.944	0.671	0.687
Mean local relief	0.517	0.944	1.000	0.769	0.833
Mean precipitation	0.522	0.671	0.769	1.000	0.851
Mean runoff	0.503	0.687	0.833	0.851	1.000
n values	Weathering	Mean	Mean local	Mean	Mean
p-values	rate	slope	relief	precipitation	runoff
Weathering rate	1.000	0.000	0.000	0.000	0.000
Mean slope	0.000	1.000	0.000	0.000	0.000
Mean local relief	0.000	0.000	1.000	0.000	0.000
Mean precipitation	0.000	0.000	0.000	1.000	0.000
Mean runoff	0.000	0.000	0.000	0.000	1.000

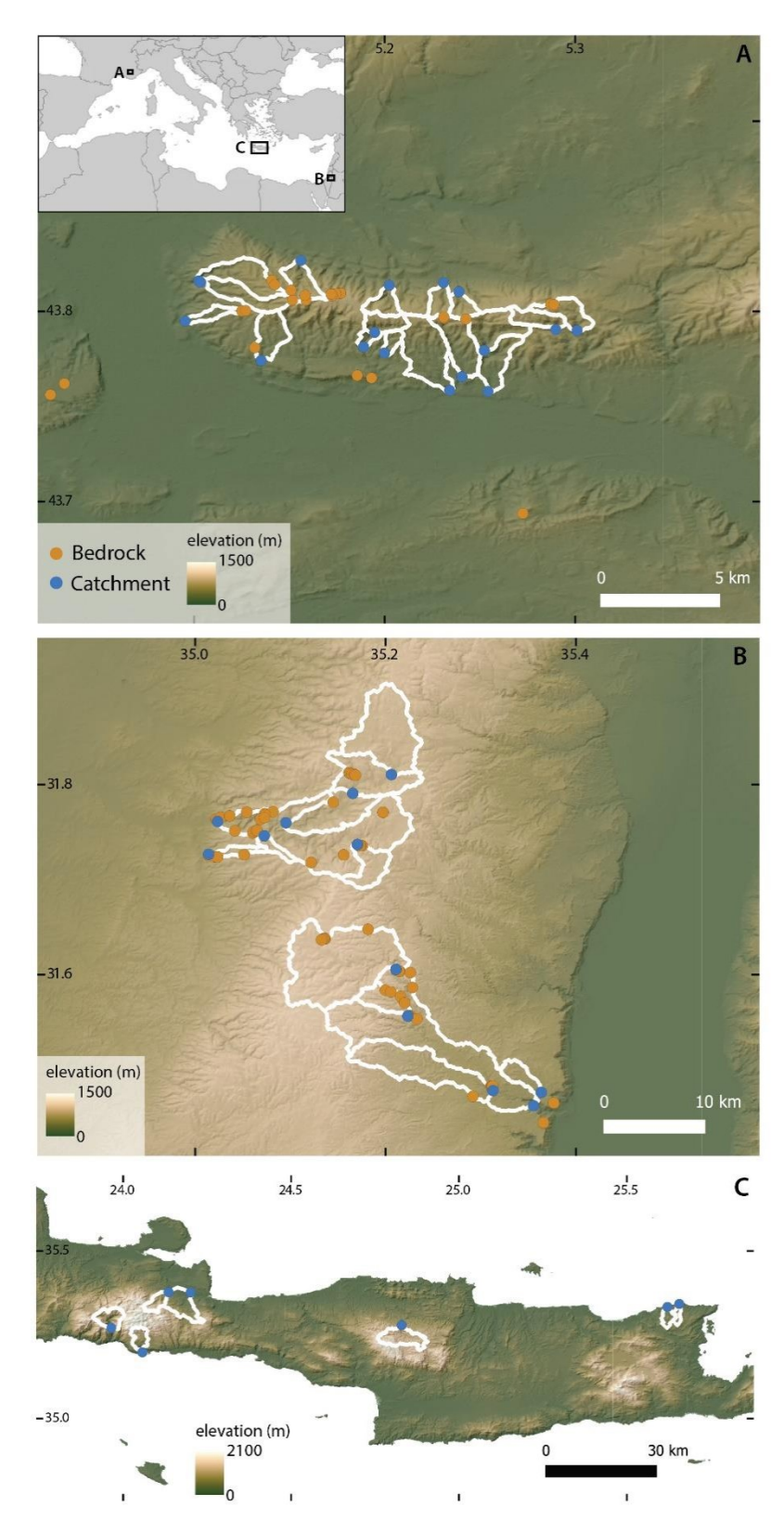


Fig. S1: Overview of catchments sampled for catchment-average denudation rates in southern France (A), Israel (B), and Crete (C), with nearby bedrock 36Cl sampling locations.

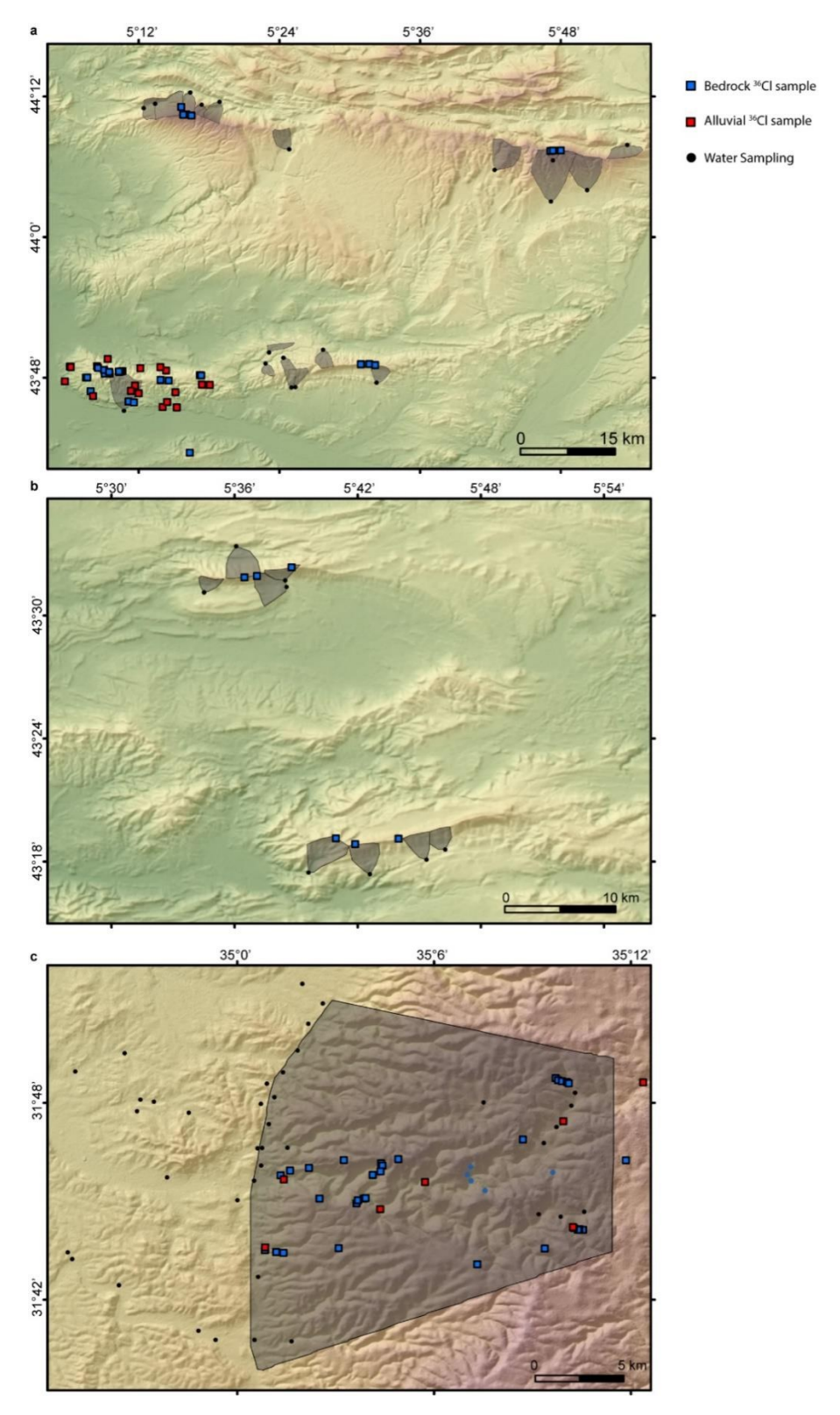


Fig. S2: Hypothetical recharge areas used to calculate the water flux required for the carbonate dissolution rate calculation for wells and springs. (a) and (b) show recharge areas for southern France, (c) for Israel, where the Western Mountain Aquifer provides the water for most wells in the coastal plain (Sheffer et al., 2010).

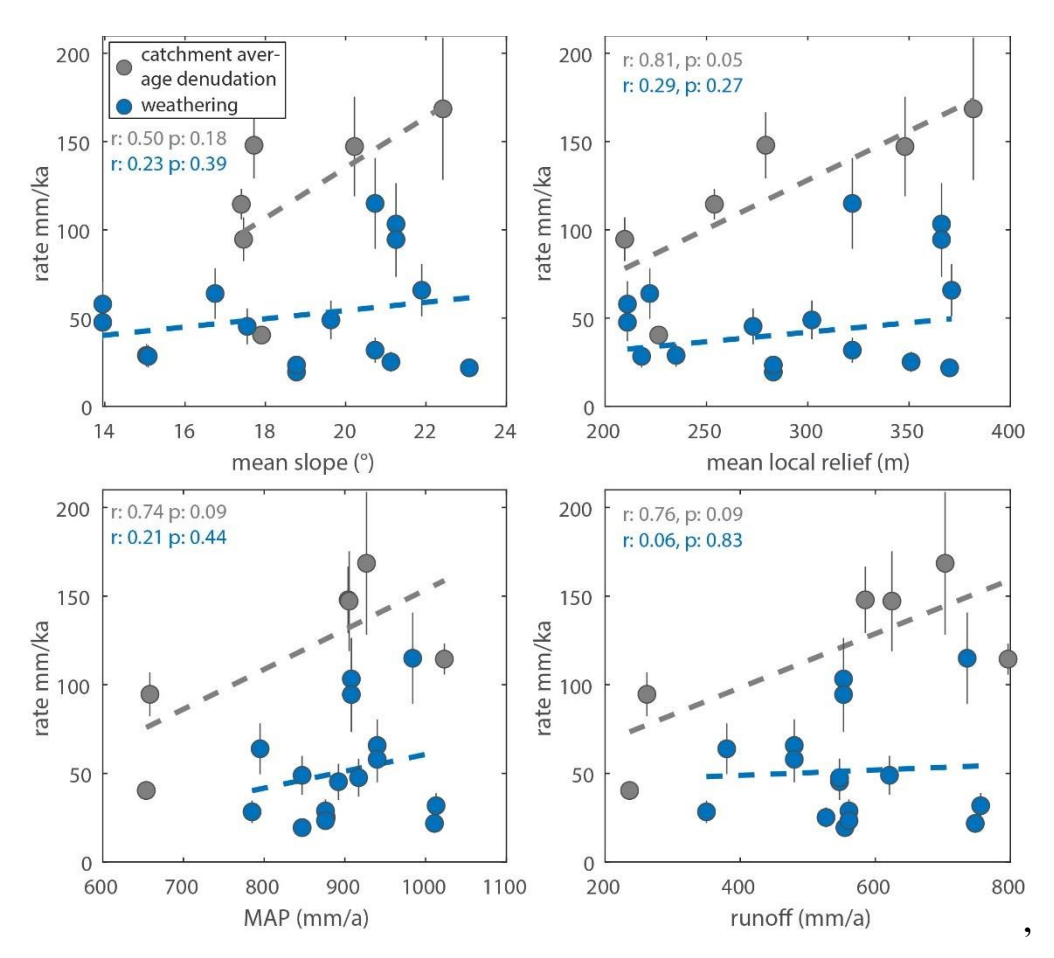


Fig S3: Correlations between catchment average 36Cl denudation rates, carbonate weathering rates, and topographic and climatic metrics for samples from Crete. Values of correlation coefficient and p-values displayed for catchment-average denudation and weathering rates.

#### References

- Avni, S., Joseph-Hai, N., Haviv, I., Matmon, A., Benedetti, L., and Team, A., 2018, Patterns and rates of 103–105 yr denudation in carbonate terrains under subhumid to subalpine climatic gradient, Mount Hermon, Israel: GSA Bulletin, v. 131, p. 899–912, doi:10.1130/B31973.1.
- Ben-Asher, M., Haviv, I., Crouvi, O., Roering, J.J., and Matmon, A., 2021, The convexity of carbonate hilltops: 36Cl constraints on denudation and chemical weathering rates and implications for hillslope curvature: GSA Bulletin, doi:10.1130/b35658.1.
- Chen, S., Mulder, V.L., Martin, M.P., Walter, C., Lacoste, M., Richer-de-Forges, A.C., Saby, N.P.A., Loiseau, T., Hu, B., and Arrouays, D., 2019, Probability mapping of soil thickness by random survival forest at a national scale: Geoderma, v. 344, p. 184–194, doi:10.1016/J.GEODERMA.2019.03.016.
- Godard, V., Ollivier, V., Bellier, O., Miramont, C., Shabanian, E., Fleury, J., Benedetti, L., and Guillou, V., 2016, Weathering-limited hillslope evolution in carbonate landscapes: Earth and Planetary Science Letters, v. 446, p. 10–20, doi:10.1016/j.epsl.2016.04.017.
- Matsushi, Y., Sasa, K., Takahashi, T., Sueki, K., Nagashima, Y., and Matsukura, Y., 2010, Denudation rates of carbonate pinnacles in Japanese karst areas: Estimates from cosmogenic 36Cl in calcite: Nuclear Instruments and Methods in Physics Research Section B: Beam Interactions with Materials and Atoms, v. 268, p. 1205–1208, doi:10.1016/j.nimb.2009.10.134 M4 Citavi.
- Ott, R.F., 2022, WeCode Weathering Corrections for denudation rates V. 1.0: GFZ Data Services, doi:10.5880/GFZ.4.6.2022.001.
- Ott, R.F., Gallen, S.F., Caves-Rugenstein, J.K., Ivy-Ochs, S., Helman, D., Fassoulas, C., Vockenhuber, C., Christl, M., and Willett, S.D., 2019, Chemical versus mechanical denudation in meta-clastic and carbonate bedrock catchments on Crete, Greece, and mechanisms for steep and high carbonate topography: Journal of Geophysical Research Earth Surface, doi:10.1029/2019JF005142.
- Ott, R.F., Gallen, S.F., and Granger, D.E., 2022, Cosmogenic nuclide weathering biases: Corrections and potential for denudation and weathering rate measurements: Geochronology Discussions, doi:10.5194/gchron-2022-5.
- Panagos, P., Van Liedekerke, M., Jones, A., and Montanarella, L., 2012, European Soil Data Centre: Response to European policy support and public data requirements: Land Use Policy, v. 29, p. 329–338, doi:10.1016/j.landusepol.2011.07.003.
- Ryb, U., Matmon, A., Erel, Y., Haviv, I., Benedetti, L., and Hidy, A.J., 2014a, Styles and rates of long-term denudation in carbonate terrains under a Mediterranean to hyper-arid climatic gradient: Earth and Planetary Science Letters, v. 406, p. 142–152, doi:10.1016/j.epsl.2014.09.008.
- Ryb, U., Matmon, A., Erel, Y., Haviv, I., Katz, A., Starinsky, A., Angert, A., and Team, A., 2014b,

- Controls on denudation rates in tectonically stable Mediterranean carbonate terrain: GSA Bulletin, v. 126, p. 553–568, doi:10.1130/B30886.1.
- Sheffer, N.A., Dafny, E., Gvirtzman, H., Navon, S., Frumkin, A., and Morin, E., 2010,
  Hydrometeorological daily recharge assessment model (DREAM) for the Western Mountain
  Aquifer, Israel: Model application and effects of temporal patterns: Water Resources Research, v.
  46, p. 251, doi:10.1029/2008WR007607.
- Thomas, F. et al., 2018, Limited influence of climatic gradients on the denudation of a Mediterranean carbonate landscape: Geomorphology, v. 316, p. 44–58, doi:10.1016/j.geomorph.2018.04.014.
- Thomas, F. et al., 2017, Morphological controls on the dynamics of carbonate landscapes under a mediterranean climate: Terra Nova, v. 29, p. 173–182, doi:10.1111/ter.12260.
- Xu, S., Liu, C., Freeman, S., Lang, Y., Schnabel, C., Tu, C., Wilcken, K., and Zhao, Z., 2013, In-situ cosmogenic 36Cl denudation rates of carbonates in Guizhou karst area: Chinese Science Bulletin, v. 58, p. 2473–2479, doi:10.1007/s11434-013-5756-8.
- Yang, Y., Lang, Y.C., Xu, S., Liu, C.Q., Cui, L.F., Freeman, S.P.H.T., and Wilcken, K.M., 2020, Combined unsteady denudation and climatic gradient factors constrain carbonate landscape evolution: New insights from in situ cosmogenic 36Cl: Quaternary Geochronology, v. 58, p. 101075, doi:10.1016/J.QUAGEO.2020.101075.